

# UNIVERSITY OF TWENTE.

**Faculty of EEMCS  
Department of Electrical Engineering  
Biomedical Signals and Systems**

---

**Assessment of daily-life dynamic interactions  
between human body and environment using  
movement and force sensing on the interface**

September 2010

Henk Kortier

---

Master thesis  
Electrical Engineering

Committee:  
Prof. dr. ir. P.H. Veltink  
dr. ir. H. van der Kooij  
dr. H.J. Zwart  
dr. ir. B.J.F. van Beijnum

---



## Abstract

This study describes different methods to evaluate the physical interaction between the human body and the environment during the performance of daily life tasks. Evaluation is performed by measuring forces and movement on the contact interface of both human body and environment. Concepts are presented for an ambulatory evaluation of task performances and estimation of body and load dynamics. Principles are demonstrated experimentally using a haptic robot, which is able to simulate loads according daily life situations. In addition, dynamics of physical mass and spring loads were estimated.

Three different arm tasks have been proposed. The first task is a reaching task: subjects had to displace different masses over approximately 23 centimeters as fast as possible within a specified endpoint accuracy. Timing and endpoint position were measured to determine the subject's task performance. Next the simulated masses were identified with an accuracy of  $\pm 4\%$ .

During the second and third task conditions, subjects had to maximize their arm velocity before the load dynamics were abruptly changed (Task 2: end effector inertia was lowered from a maximum of 25 kg to 2 kg. Task 3: Viscous damping was raised from 10 to 300 Ns/m ). Task performances were evaluated by the applied impulse, i.e. multiplication of simulated end-effector inertia with its velocity at the onset of change in load dynamics.

Full identification of body dynamics was impossible as the duration of body perturbations was too short. However responses were visible when load dynamics suddenly changed. Condition 3 showed under-damped responses in the recorded interface forces which could be caused by a high muscle stiffness.

Experiments with the haptic robot gave partially erroneous results in identified parameters which were probably caused by rendering limitations and wear in actuators and/or gearboxes. Estimation with physical loads were accurate within 5% for mass loads and 3% for spring loads. In contrast to simulated loads with the haptic robot, parameter estimations were successfully estimated by a recursive identification algorithm.

## **Preface**

This report represents the final thesis for completing my Master of Science study in the field of Electrical Engineering. I would like to thank some people for their support during this assignment. First I would like to thank my daily supervisor Peter Veltink for all the effort he has put in helping me to complete this assignment. Furthermore I would like to thank the other committee members: Herman van der Kooij, Hans Zwart and Bert-Jan van Beijnum for their support.

Enschede, September 9, 2010

# Contents

<b>1. Introduction</b>	<b>1</b>
1.1. Context . . . . .	1
1.2. Research problem . . . . .	3
1.2.1. Measuring forces and estimating movement . . . . .	3
1.2.2. System identification . . . . .	3
1.3. Research aims . . . . .	5
1.4. Thesis outline . . . . .	5
<b>2. Background information</b>	<b>7</b>
2.1. Interacting systems . . . . .	7
2.2. Evaluation of human body dynamics . . . . .	7
2.2.1. Identification of musculo-skeletal systems . . . . .	7
2.2.2. Optimal execution of arm tasks . . . . .	10
2.2.3. Conclusions of background information in the evaluation of human body dynamics . . . . .	13
2.3. Modeling physical loads . . . . .	13
2.4. Parametric system identification . . . . .	15
2.4.1. Linear regression . . . . .	15
2.4.2. Prediction error method . . . . .	16
2.4.3. Subspace method for state space models . . . . .	17
2.4.3.1. Comparison Prediction Error and Subspace method . . . . .	18
2.4.4. Recursive identification . . . . .	19
2.4.4.1. Recursive algorithm . . . . .	19
2.5. Non parametric identification . . . . .	21
2.5.1. Frequency response models . . . . .	21
2.5.2. Impulse response models . . . . .	21
2.5.3. Closed loop identification . . . . .	22
2.5.3.1. Direct approach . . . . .	22
2.5.3.2. Indirect approach . . . . .	22
2.5.3.3. Joint input-output approach . . . . .	23
2.5.4. Identification of physiological meaningful parameters . . . . .	23
2.5.4.1. Discrete to continuous domain conversion . . . . .	23
2.5.5. Model Validation . . . . .	24
2.6. Conclusions of discussed identification algorithms . . . . .	25

<b>3. Methods</b>	<b>27</b>
3.1. Daily life tasks . . . . .	27
3.1.1. Displace object: Minimal duration . . . . .	27
3.1.2. Throw object: Maximal momentum . . . . .	28
3.1.3. Punch object: Maximal momentum . . . . .	28
3.1.4. Task summery . . . . .	28
3.1.5. Identification requirements . . . . .	28
3.1.6. Load disturbances . . . . .	29
3.2. Experimental setup . . . . .	29
3.2.1. Comparison of appropriate setups . . . . .	29
3.2.2. HapticMASTER . . . . .	30
3.2.3. Additional devices. . . . .	31
3.3. Experimental protocol . . . . .	31
3.3.1. Protocol . . . . .	33
3.3.2. Signal Processing . . . . .	34
3.3.2.1. Force en movement signals . . . . .	34
3.3.2.2. Frame alignment . . . . .	36
3.3.2.3. Evaluation of task performance . . . . .	37
3.3.2.4. Identification of simulated dynamics . . . . .	37
3.4. Physical load experiments . . . . .	38
<b>4. Experimental evaluation results</b>	<b>41</b>
4.1. Evaluation hapticmaster's performance . . . . .	41
4.2. Displace Object task, simulated mass . . . . .	46
4.2.1. Evaluation of task performance . . . . .	46
4.2.2. Identification of system dynamics . . . . .	47
4.3. Throw Object task, abrupt reduction of simulated mass . . . . .	54
4.3.1. Identification of system dynamics . . . . .	54
4.4. Punch object task, abrupt rise in simulated viscous damping . . . . .	59
4.4.1. Identification of system dynamics . . . . .	60
4.5. Physical mass and spring load tasks . . . . .	64
<b>5. Discussion and Conclusions</b>	<b>67</b>
5.1. Evaluation of task performance . . . . .	67
5.2. Identification of load dynamics . . . . .	68
5.2.1. Changing load dynamics . . . . .	69
5.2.2. Estimation error analysis . . . . .	70
5.3. Identification of body dynamics . . . . .	71
5.3.1. Relation between responses of changing loads and movement control of the human body . . . . .	72
5.4. Conclusions . . . . .	73
5.5. Recommendations . . . . .	73

<b>A. HapticMASTER related</b>	<b>75</b>
A.1. Control interface window . . . . .	75
A.2. HapticMASTER Specifications . . . . .	75
<b>B. Additional information</b>	<b>77</b>
B.1. Derivation of vd Helm's upper arm model . . . . .	77
B.2. Kalman Approach for recursive identification . . . . .	78
<b>References</b>	<b>79</b>



# 1. Introduction

## 1.1. Context

The STW 'PowerSensor' project is an ongoing research program at the University of Twente. The objective of the project is to develop modalities for quantitative assessment of dynamic interaction between the human body or robot, and the environment. Application areas one can think of include physical labour, rehabilitation and sports. Many tasks require an optimal or improved dynamic interaction. It is therefore essential to assess the interaction quantitatively in terms of task performance, forces and movement at the interfaces, power transfer, timing and work done. Assessment of the functional task performance by means of a cost function requires suitable criteria, e.g. duration, smoothness or momentum of the movement. Next the therapist can give quantitative feedback about the condition of a patients who, for example, suffer from Parkinson's disease or have had a stroke. Other applications in sports allow feedback of coaches to their athletes, for example in shot-put, discus throw, but also in sports where interaction with stationary objects (e.g. solid ground) occur, for example high and long jump. In addition, estimation of effective dynamics of the human or robot and environment during the execution of functional tasks performed in daily life gives major information about the task conditions.

Figure 1.1 shows a conceptional drawing of the 'PowerGlove'. Realization of the 'PowerGlove' is one of the objectives within the 'PowerSensor' project. The glove is instrumented with multiple miniature powersensors. A single powersensor measures forces and movement at the interface of human hand and load.

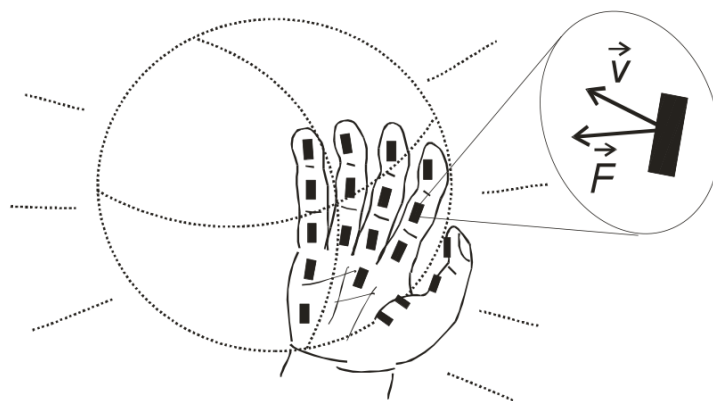


**Figure 1.1.:** PowerGlove concept. The glove is instrumented with miniature powersensors. A powersensor measures movement and forces at the interface of hand and load. The power transfer is subsequently determined by the product of forces and velocities

Energy flows between multiple interacting systems can be described and illustrated by a bondgraph diagram. In figure 1.2 a bondgraph of an interacting human body with environment is shown. This bondgraph can be transformed to a block diagram which is visualized in figure 1.3. Because the causality is not fixed, two diagrams are possible. The human body can therefore act as an impedance or admittance controller.

System dynamics are described by the quotient of effort and flow variables, in the mechanical domain represented by respectively forces and velocities, and will therefore behave as an impedance ( $Z$ ) or admittance ( $Y$ ):

$$Z = \frac{1}{Y} = \frac{\mathbf{F}}{\mathbf{v}} \quad (1.1)$$

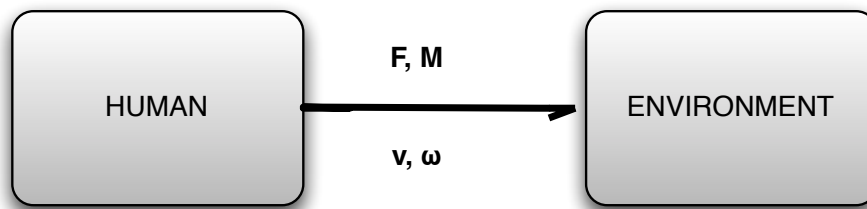


**Figure 1.2.: Bondgraph diagram** - Human interaction with the environment can be visualized by a bondgraph diagram. In the mechanical domain efforts are described by forces and momenta whereas flows are described by velocities and angular velocities. Their inner product gives the power transferred between both elements. Direction of positive energy flow is denoted by the half arrow. In the case of passive loads, the human delivers power and the connected load will absorb. A causality mark is not given as it is obviously not predefined in human environment interaction.

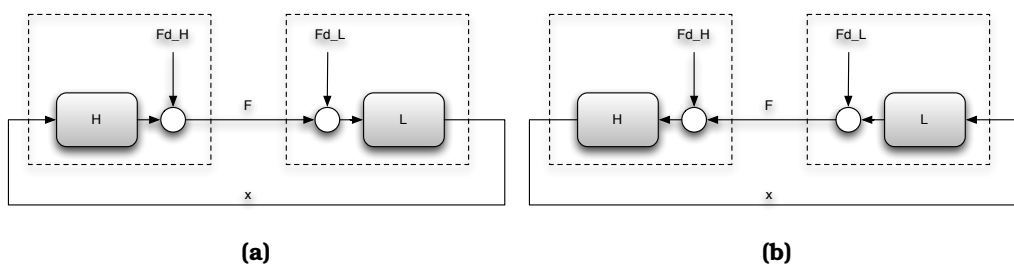


**Figure 1.3.:** Closed loop block schemes of human-environment interaction. H = human dynamics, L = Load dynamics, F = Force, x = Position, Fd.H = Internal body force disturbances, Fd.L = Load force disturbances. Two control perspectives are possible: (a) load = impedance and human = admittance. (b) load = admittance and human = impedance.

## 1.2. Research problem

### 1.2.1. Measuring forces and estimating movement

Forces exerted at the interface of two interacting bodies, combined with the movement they undergo, characterize the effective dynamics of both bodies. Sensing interaction forces and moments is possible by three dimensional force sensors which are widely commercially available (1). Unfortunately these sensors do have a relatively large package size and mass and are therefore unsuitable for applications where millimeter scale is desired. Development of a new miniature triaxial force sensor is part of the STW "PowerSensor" project.

The ability to reconstruct movements during free motions at the interface between body and environment, applying small micro-machined 3D inertial sensors (accelerometers and gyroscopes), possibly combined with magnetometers have been developed recently (2). However for accurate reconstruction of specifically velocities, positions, angular velocities and orientations, one has to deal with the restriction that the arbitrary movement should be limited in duration (typically several seconds). Fortunately, most human interactions with the environment are of limited duration or approximately cyclical. Hence such conditions can be used to avoid integration drifts.

### 1.2.2. System identification

Common system identification techniques demand a linear and stationary system such that it can be identified properly. Furthermore, it is required that input(s) and output(s) terminals are directly accessible in open loop. None of these requirements are met when a dynamical system is interacting with the human body! The musculoskeletal system is highly nonlinear, the human body has the opportunity to adapt to changes of the interacting dynamics and finally a healthy human body interacts in a closed loop condition. In addition, load dynamics can change over time.

Joint system dynamics of closed loop systems are only identifiable when sufficient force and movement information on the interface of contact has been obtained. Identification of dynamics of subsystems inside the closed loop require dynamic knowledge of other subsystems inside the loop, also called the indirect approach for closed loop identification (3). Prior knowledge of human body and load in human environment interaction is often unavailable, therefore other identification algorithms should be used for proper identification of closed loop parts. The joint In-Output approach (3) uses a known external disturbance for identification. Cross spectral densities of the disturbance signal and systems in and output signals can be used to form a spectral estimator of the system.

Regarding the closed loop configuration in figure 1.3, disturbances generated by the load give information about the human body and disturbances generated by the body give information about the load it is interacting with.

## Task Execution

During many functional tasks, for example displacing a cup coffee, human body dynamics will be more variable than dynamics of the load the body is interacting with. The load will be periodically stationary, whereas dynamics of the human body are continuously adapting for optimal execution of the specified task. It will use patterns gathered by learning the task and hence make use of feedforward control for execution of the task. The load is perturbed by internal force disturbances of the human body (see figure 1.3a), mainly caused by muscle contractions. Internal load disturbances will be minimal during execution, only when its dynamics change over time, e.g. when collision occurs, the body will be perturbed. This leads us to the implication that information obtained by force and movement sensors at the interface, mainly gives the force/movement relation of the load. Moreover the load generally has a relatively small frequency characteristic, which makes it more easy to identify the particular load.

One can conclude that humans often practice the actor role and that loads often behave passively. This implies that in most cases of interactions with the environment, causality is applied by the human body (see figure 1.3a).

This implication is in contrast to other task classes like minimizing position deviations while being disturbed, e.g. driving a car on a bumpy road. Now an external (load) disturbance is applied to the body. The body will behave piece-wise stationary and has a relatively small frequency characteristic compared to the load disturbance. In case when external disturbances are exactly known and the human dynamics are approximately stationary, human body dynamics are possibly identifiable (see (4) and (5)).

Because former types of task classes appear more frequently in daily life activities, it is obviously more appealing to evaluate the human body task execution by performance criteria, rather than trying to identify its dynamics. This approach has also been studied by Körding and Wolpert (6) and by Todorov and Jordan (7).

### 1.3. Research aims

#### Research question

What information can be derived about the dynamics of human body and load and about task performance from force and movement measured on the interface?

#### Hypothesis

- Load dynamics can be identified during stationary periods if perturbation is sufficiently exciting the load dynamics.
- Task performance can be evaluated.
- Momentary information about human dynamics can be derived from responses to changing load characteristics.

Research in this masters thesis is conducted in multiple parts, which have been summarized by the research question. All parts share the feature that the information to be processed is gathered by a combination of force and inertial (generally accelerometer) sensors, positioned on the interaction interface of two bodies. The relation of sensed quantities will be used as input for the algorithms to be developed.

This research work has been focused on a specific class of interactions between human body and environment. In short, this class can be defined as:

- Functional movement tasks with specific conditions and criteria
- Piecewise stationary passive environmental loads

### 1.4. Thesis outline

Chapter 2 starts with a class definition of daily life tasks which will be treated throughout this research work. Then a literature study is given and different algorithms in the field of system identification are discussed. Chapter 3 describes the experimental method. First different tasks are explained which will be performed during the experimental setup. Then an appropriate setup is selected and a measurement protocol is given. Next Chapter 4 gives the results for all experiments. A clear distinction should be made between results with simulated dynamics and those of the real physical loads. Final chapter discusses the results and give conclusions of this research work. In addition recommendations are given for further work.



## **2. Background information**

This chapter describes the background of the assignment. Inspiration for methods and experimental setups are derived from this literature study. First a class will be defined where the proposed human load interactions belong to. Next section treats background information of the evaluation of human body dynamics. Final section describes common algorithms in the system identification field which are applicable to this research work.

### **2.1. Interacting systems**

As mentioned in the global introduction, this research work is focused on a particular class of interactions. Piecewise stationary passive loads, which can be expressed with linear second order dynamics, are considered.

Dynamics of the human arm can, only in very specific situations, be described as stationary and linear. In general, the system is highly adaptive and non linear when operating in daily life situations. In this situation it is more convenient to characterize interactions with a second system with a bondgraph description, as shown in figure 1.2.

Now, when force or movement perturbations are imposed on either system 1 (e.g. human body) or system 2 (e.g. environmental load), the other coupled system will be excited and movement or force transients become available at the interface. Hence perturbations in system 1 give information about system 2 and vice versa.

### **2.2. Evaluation of human body dynamics**

This subsection summarizes related work in the field of system identification of musculo-skeletal systems (in particular: identification of arm/hand dynamics). Thereafter, work in the field of optimal task execution will be outlined.

#### **2.2.1. Identification of musculo-skeletal systems**

Dynamics of joint mechanics are a fundamental characteristic of the human motor system. They determine the displacements evoked by perturbing forces that must be generated to perform a voluntary movement. Different research studies have been performed in the field of identification of musculo-skeletal systems.

Because this research work is treated within the 'PowerSensor' context, the stress falls on identification of arm and hand dynamics.

First step in system identification is the choice of model structure that captures the dynamics of interest. The many degrees of freedom and high redundancy of arm movements and manipulations cause tremendous difficulties in modeling. Hence it will be cumbersome to model the entire musculoskeletal system of the upper arm. Therefore research groups (for example in (4),(8) (9)) often choose for a one dimensional abstraction of the upper arm. Moreover Wolpert (10) demonstrated that for optimal task execution redundant degrees of freedom are not optimized unless they are relevant for the task performance.

The musculo-skeletal system of the human arm has two mechanisms which contribute to the total generated force. The first one is based on intrinsic properties such as mass, damping and stiffness. The second mechanism is formed by reflex loops with muscle spindles providing sensory information on muscle stretch and stretch velocity, and Golgi tendon organs providing sensory information of active muscle force.

Different research groups successfully identified dynamics of the human arm and succeeded in separating both mechanisms. The group of van der Helm et al. (4), (11) used a frequency domain identification approach. External force perturbation were applied to the hand, which was constrained to allow only minimal one dimensional positional deviations. In this condition the arm and hand dynamics are considered to be linear. The suggested upper arm model is given in figure 2.1b. The arm model consists of, intrinsic arm  $H_i$  and hand dynamics  $H_h$  (figure 2.1a), reflexive length and velocity feedback  $H_r$  and activation dynamics  $H_{act}$ . The mentioned musculo-skeletal model is only valid in situations where the arm dynamics are considered to be linear and piece-wise stationary, which is often not the case in daily life functional tasks.

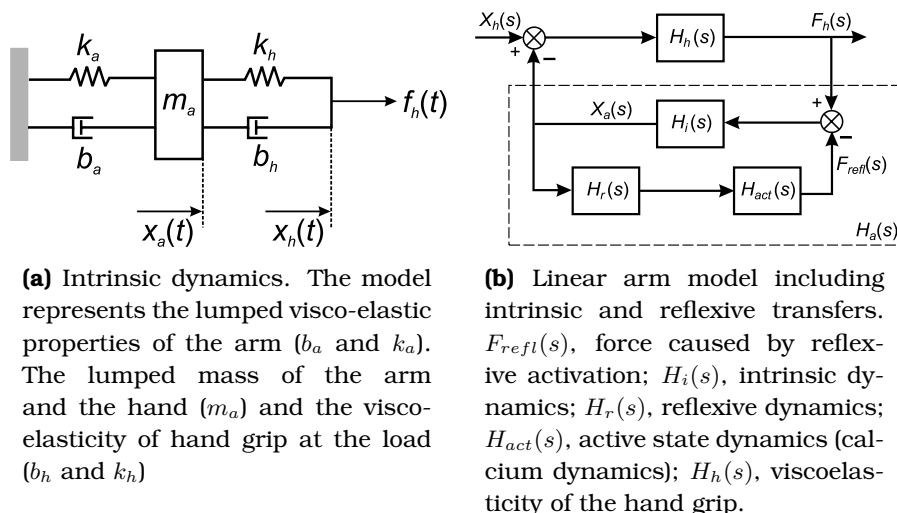


**Figure 2.1.:** Model of arm dynamics as suggested by van der Helm (4). A derivation of the proposed model can be found in the appendix B.1

Reflex dynamics are considered negligible when using wide band disturbances. Now when using small band perturbations both mechanisms can be distinguished.

Since the experiment is performed in closed loop, a joint-input-output approach (discussed in section 2.5.3.3) is used for a correct estimation of arm dynamics. This method has been extended to (multidimensional) planar movements in (12) and (13).

Kearney et al. (5) successfully separated both force contributions by a time domain approach. Prior knowledge about the occurrence of the reflexive dynamics (after 40 ms) is used to subtract the intrinsic part from both components which results in the reflexive part.

Other less successful separation of both contributions include the modulation of EMG activity (5). However, these studies have had little success in characterizing the contributions of reflex activity to the mechanical response. Possible explanation was found to be the strongly inherent nonlinear behavior of the reflexive part which can not be modeled by quasilinear modeling methods.

Applied identification of the human arm has been done by Pick and Cole (14). Dynamic properties of a driver's arm holding a steering wheel that is subjected to random torque disturbances are investigated. Identification of passive dynamics were successful, despite the multiple freedoms of the arm. A similar identification method to that of van der Helm was used. Unfortunately, the measurement instrumentation was not so well which resulted in bad SNR ratios. Hence identification was not good enough to identify reliable reflex contributions.

Yangming and Hollerbach (15) presented a method to estimate the time varying compliance parameters of the elbow joint from single movements. They developed a nonrestrictive 2D airjet system where perturbations can be applied to the human joints continuously, without impairing the natural movement. This significant advance in apparatus brings the possibility of identifying the time-varying human joint mechanical properties under natural movement. Due to the limited power in the high-frequency region of the perturbation and the error introduced by high-pass filtering, the method only works for slow time-varying movements.

Xu and Hollerbach (16) extended above method using an ensemble method. Ensemble methods are promising because the results at any instance are supported by more data points. The suggested method had few major advantages: it is robust to inter-trial variation, it can handle reasonably fast time-varying dynamics, only a few restrictions are placed on the input signal and the error due to the method itself can be characterized. Disadvantage is that many trials are required in order to obtain a reliable estimation. However for cyclic arm movements, (e.g. during walking) it is promising.

Konczak and Bromman (17) presented an identification methods without use of a continuous external perturbation source. The algorithm was able to track parameter variations with the assumption that they vary slowly in time. During single-joint motions the average trajectories change monotonically or at low frequency. Muscle

dynamics may take on the form of a low-pass filter in simple movement tasks, thus preventing high-frequency changes of muscle related damping and stiffness.

Fairly good results were obtained but the authors clearly state that when external perturbations are used identification can be improved significantly. Disadvantage is that movements are strictly restricted around the elbow joint, furthermore knowledge of load dynamics is essential.

### 2.2.2. Optimal execution of arm tasks

Many human arm movements task in daily life can be achieved in a large number of ways, thus the exact movement executed at a particular time is not completely determined by the motor task. In addition, we are able to produce appropriate movements in tasks that involve almost arbitrary combination of constraints: avoidance or pass through locations, exert force at specific time, speed requirements, etc.

As a consequence, extensive research has been done in the field of motor control, mostly by observational studies. This is clearly a different approach to evaluate the human body compared to estimating dynamics of musculo-skeletal systems as described in the previous section. Regarding our defined class of functional environmental interactions, it is more intuitive to quantify task performances of the human than estimating its dynamics!

Part of the traditional observational studies was the identification of biological regularities. Once this had been done, structures were derived that produces them. Examples include: Fitts law (see formula 2.1 and 2.2), bell-shaped velocity profiles of reaching movements, and the relation between the velocity of end-effector trajectory and the geometric path it describes (described as 2/3 power law, see formula 2.3) (18).

Fitts law (19) gives a prediction of the time required to rapidly move to a target area as function of the distance to and the size of the target. In mathematical notation:

$$T = a + b \text{ ID} \quad (2.1)$$

Where ID is called the index of difficulty (ID), and has units of bits. It gives an indication of the task's difficulty. Here,  $T$  is the average time taken to complete the movement,  $a$  can be thought as the reaction time between awareness of the endpoint point position and the onset of movement, and  $b$  as the inverse of the user throughput, i.e. the number of bits the user can handle per second. Hence  $b$  has the units of time per bit. ID can be expressed as:

$$\text{ID} = \log_2\left(1 + \frac{D}{W}\right) \quad (2.2)$$

Where  $D$  is the distance from the starting point to the center of the target and  $W$  is the width of the target measured along the axis of motion.

The '2/3 power law' was a result of observations by Lacquaniti et al. (20). It states that the angular endpoint velocity is proportional to the curvature of the endeffector path by satisfying the power relation:

$$V(t) = KR(t)^{(2/3)} \quad (2.3)$$

Where  $V$  is angular end-point velocity,  $K$  is a constant gain factor and  $R$  is the curvature of the endeffector path.

Flash and Hogan (21) were the first researchers who proposed a mathematical model, called 'minimum jerk model' to describe observed voluntary arm movements and comply with derived structures (e.g. Fitts law). The minimum jerk model is formulated by defining the following objective function, a measure of performance for any possible movement: square of the jerk (rate of change of acceleration) of the hand position integrated over the entire movement.

Uno et al (22) expand this model from the viewpoint emphasizing the dynamics of the controlled object and proposed a mathematical model which is also comprising the dynamics of the arm, 'minimum torque-change'. A mathematical model, defined as an objective function  $C_T$ , gives a measure of performance for any possible movement.

$$C_T = \frac{1}{2} \int_0^{t_f} \sum_{i=1}^n \left( \frac{dz_i}{dt} \right)^2 dt \quad (2.4)$$

where  $z_i$  is the torque generated by the  $i$ -th actuator,  $t_f$  is the movement time.

Todorov and Jordan developed (18) a new model that essentially combines the appealing features of bell-shaped velocity profiles and inverse relationship between curvature and speed of curved hand movements (2/3rd power law).

For a linear system the minimum time requirement for a certain reach movement results in 'bang-bang' control, where the control signal is instantaneously switched between its maximum positive and negative values to accelerate and decelerate. However, 'bang-bang' control hardly results in observed bell-shaped velocity profiles. Furthermore, these models do not give a principled explanation why the central nervous system should have evolved to optimize such quantities (jerk or torque), other than they predict smooth trajectories.

Wolpert et al. (23) first proposed that the central nervous system (CNS) internally simulates the dynamic behavior of the motor system in planning, control, and learning by an internal model. Using an experimental study they showed that the CNS combines sensory inflow (proprioception) and motor outflow (commands sent to the arm) to estimate the current states (velocity and position) of the hand. Next they developed a model based on the kalman observer framework, to verify the observed CNS behavior. They state that the CNS uses a forward model to estimate the location of the hand in space.

A few years later, Wolpert and Harris (24) presented a unifying theory of eye and hand movements based on the assumption that the neural control signals are corrupted by noise whose variance increases with the size of the control signal. Noise in the final neural control signal will cause trajectories to deviate from the desired path. Noise will accumulate over time, leading to variability in final position.

Again a few years later, Todorov and Jordan provided in a new theory for motor coordination based on optimal feedback control (7). They capture the signal dependent noise feature and optimal feedback controller. Most important of their approach is the application of optimization techniques to find the feedback control law that minimizes error in task performance. The authors use, what they call, the ‘minimum intervention principle’ which postulates that deviations from an average trajectory are only corrected if they interfere with the task performance. A diagram is shown in figure 2.2

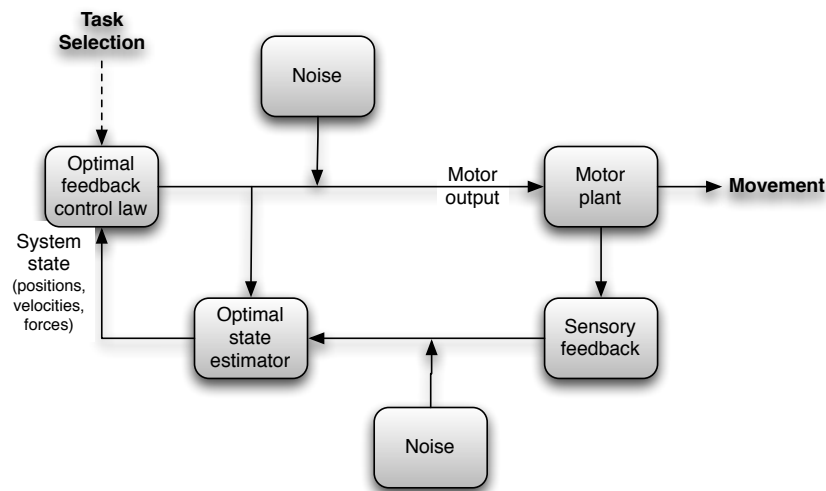


**Figure 2.2.:** Optimal feedback control as proposed by Todorov and Jordan (7). The optimal feedback control law is selected by the CNS based on the specific task. An optimal state estimate is based on sensory feedback (delayed and noisy), efferent copy of prior control signals and forward internal models. Adapted from (25)

More recently, researchers showed that that the brain uses a bayesian control strategy to execute motor tasks (6) (26) and (8). When learning a new motor skill both sensor and task possess variability. According to the Bayesian theory an optimal estimate of new states results from combining information about prior state distributions with sensory feedback. By experiments and models it is shown that the CNS employs probabilistic models during sensorimotor learning. Todorov developed an algorithm for the stochastic optimal controller where signal dependent noise and Bayesian probabilistic theories are integrated (9). Which is in essence an updated version of (24).

### 2.2.3. Conclusions of background information in the evaluation of human body dynamics

Background literature of two distinct approaches in evaluating dynamics of the human body, have been described. First is the identification of underlying musculo-skeletal arm dynamics. Because two mechanisms contribute to the arm dynamics, assessment of full arm dynamics is only possible when the arm is restricted to minimal positional deviations (linear operating point) and excited by known external perturbations.

However many arm tasks in daily life are performed in situations in which these requirements are in no way achievable. Therefore a different approach which deals with modeling of the functional arm task, has been reviewed. This concept is intuitively a more attracting method to judge the task performance of a subject. Only the task goal will be criticized. Underlying musculo-skeletal mechanisms determine only partially the performance of tasks.

## 2.3. Modeling physical loads

Environmental loads are regarded to be linear during one or a finite number of periods while interacting with the human hand. Therefore a linear stationary physical environmental load can be modeled as a second order equation comprising a mass, a spring and a damper.

A configuration example is illustrated in figure 2.3. The system can be mathematically described with a well known linear second order differential equation:

$$m\ddot{x} + b\dot{x} + kx = F \quad (2.5)$$

Where  $m$ ,  $b$  and  $k$  correspond to respectively mass [kg], damping constant [Ns/m] and spring constant [N/m]. In addition  $x$  represents the position and  $F$  an external force input.

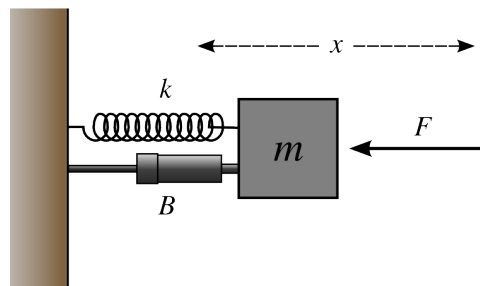


**Figure 2.3.:** Mass Spring Damper configuration system with external force input.

Next the following parameters are defined, where  $\omega_0$  [rad/s] is the undamped natural frequency, and  $\zeta$  is called the damping ratio which is dimensionless. These

equation are more general as they are applicable in multiple domains (e.g. electrical/ mechanical/ chemical).

$$\omega_0 = \sqrt{\frac{k}{m}} \quad \zeta = \frac{d}{2\sqrt{mk}} \quad (2.6)$$

Conversion to the Laplace domain gives the load dynamics  $H_l(s)$ :

$$H_l(s) = \frac{1}{ms^2 + bs + k} \quad (2.7)$$

$$= \frac{K\omega_0^2}{s^2 + 2\zeta\omega_0s + \omega_0^2} \quad (2.8)$$

These descriptions of a second order system are in transfer function form, alternatively one could write them using a state space description:

$$\begin{bmatrix} \dot{\mathbf{x}} \\ \dot{\mathbf{v}} \end{bmatrix} = \begin{bmatrix} 0 & 1 \\ -k/m & -b/m \end{bmatrix} \begin{bmatrix} \mathbf{x} \\ \mathbf{v} \end{bmatrix} + \begin{bmatrix} 0 \\ 1/m \end{bmatrix} f(t) \quad (2.9)$$

$$\mathbf{y} = [1 \ 0] \begin{bmatrix} \mathbf{x} \\ \mathbf{v} \end{bmatrix} + [0] f(t) \quad (2.10)$$

This corresponds to the general state space description:

$$\dot{\mathbf{x}} = \mathbf{Ax} + \mathbf{Bu} \quad (2.11)$$

$$\mathbf{y} = \mathbf{Cx} + \mathbf{Du}$$

Where  $\mathbf{x}$  are the states,  $\mathbf{u}$  are the inputs,  $\mathbf{y}$  are the outputs,  $\mathbf{A}$  is the state matrix,  $\mathbf{B}$  the input matrix,  $\mathbf{C}$  is the output matrix and  $\mathbf{D}$  is the forward matrix.

## 2.4. Parametric system identification

System identification deals with the problem of building mathematical models of dynamical systems based on observed data obtained from the system.

The first step in the identification process is definition of a model structure of the system to be identified. A general system structure is given in figure 2.4.

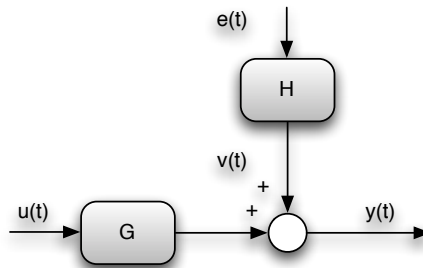


**Figure 2.4.:** System description. With  $u$  the input,  $y$  the output,  $e$  white gaussian noise and  $v$  colored noise.  $G$  and  $H$  represent respectively the system and noise model.

The model structure shows the following relation between measured output  $y$  and input  $u$ :

$$y(t) = G(z)u(t) + H(z)e(t) \quad (2.12)$$

The output  $y(t)$  is an addition of the actual system  $G$  output and unmeasurable disturbance  $v(t)$ . This disturbance term will be modeled using the transfer function  $H$  and white noise term  $e$ . The system ( $G$ ), and disturbance model ( $H$ ) are supposed to be described in the  $z$ -domain. This also implies that input, output and noise signals are to be sampled. It has to be stressed that it is certainly not guaranteed that a real system fits into this structure. Important requirement is that the disturbance  $v(t)$  and input signal  $u(t)$ , are uncorrelated.

The following subsection give an overview and show fundamental relations between measured output and input. In addition, it will show the least squares solution, which is applicable for particular model structures, and one of the solutions to estimate a model of the system  $G$ .

Additionally three other identification methods which are suitable with respect to this research topic, will be outlined briefly. These include a subspace method, prediction error method and finally a recursive method.

### 2.4.1. Linear regression

Linear regression model structures are very useful in describing basic linear and non linear systems. The linear regression employs a predictor that is linear in the parameter space  $\theta$ :

$$\hat{y}(t|\theta) = \varphi^T(t)\theta \quad (2.13)$$

Here  $\varphi$  is the regression vector, i.e. for an ARX (Auto-Regression with eXogeneous inputs) structure:

$$\varphi(t) = [-y(t-1) \dots -y(t-n) \ u(t-1) \dots u(t-m)]^T \quad (2.14)$$

where  $u(t)$  and  $y(t)$  are the system's input and output at time  $t$ . Furthermore the parameter vector  $\theta$  is given by:

$$\theta = [a_1 \dots a_n \ b_1 \dots b_m]^T \quad (2.15)$$

with equation 2.13 the prediction error becomes:

$$\epsilon(t, \theta) = y(t) - \varphi^T(t)\theta \quad (2.16)$$

Next the least-squares criterion function is defined as (27) :

$$V_t(\theta) = \sum_{k=1}^t [y(k) - \varphi^T(k)\theta]^2 \quad (2.17)$$

The unique feature of this criterion is that it is a quadratic function in  $\theta$ . Therefore, it can be minimized analytically, which gives, provided the indicated inverse exists:

$$\hat{\theta}_t^{LS} = \left[ \sum_{k=1}^t \varphi(k)\varphi^T(k) \right]^{-1} \sum_{k=1}^t \varphi(k)y(k) \quad (2.18)$$

Which is the least-squares estimate (LSE) or in more general terms (3):

$$\hat{\theta}_t = R^{-1}(t)f(t) \quad (2.19)$$

$$R(t) = \sum_{k=1}^t \varphi(k)\varphi^T(k) \quad (2.20)$$

$$f(t) = \sum_{k=1}^t \varphi(k)y(k) \quad (2.21)$$

### 2.4.2. Prediction error method

This is a class of identification algorithms where the predicted model output is compared to actual measured system output. Next the algorithm anticipates to the prediction error which is the difference between modeled and measured system outputs. In mathematical notation this can be expressed by a cost function which have to be minimized:

$$V_t(\theta) = \sum_{k=1}^t \|\epsilon(k, \theta)\|^2 \quad (2.22)$$

with:

$$\epsilon(k, \theta) = y(k) - \hat{y}(k) \quad (2.23)$$

The general considered model is depicted in figure 2.4. Goal of identification is to determine the process model  $G$  from measured in and output data which requires

knowledge of the noise model  $H$  (3). These models will be written as function of the parameter vector  $\theta$ . By varying the parameters the transfer functions will be tuned to match the assumed process and noise models. A perfect match results in a white noise prediction error. In practice tuning is carried out by minimizing the error  $\epsilon$  with a least squares fit.

We already mentioned the ARX model structure in equation 2.14. The structure can be described as a rational function:

$$G(z, \theta) = \frac{B(z, \theta)}{A(z, \theta)} \quad \text{and} \quad H(z, \theta) = \frac{1}{A(z, \theta)} \quad (2.24)$$

As the equation indicate, both system and noise model share the same denominator. It may be questioned whether a real model fits into this structure, but the large advantage of this structure is the linearity in the parameters. That is clearly an advantage as it means that e.g. linear least squares techniques can be applied to obtain the parameter estimate.

This is in contrast to model structure like ARMAX, output error (OE) and Box-Jenkins (BJ), where the noise model does not have the same denominator as the process model. Noise models can be estimated more accurately but the model structure require a non linear iterative optimization technique, like the 'Gauss-Newton' or 'Levenberg-Marquardt' algorithms(3).

### 2.4.3. Subspace method for state space models

Other possible identification technique is the so called subspace method. The mathematical background of this technique is more complicated and will be outlined briefly.

The innovation form of state space equations are described by:

$$\mathbf{x}(t+1) = A\mathbf{x}(t) + B\mathbf{u}(t) + K\mathbf{e}(t) \quad (2.25)$$

$$\mathbf{y}(t) = C\mathbf{x}(t) + D\mathbf{u}(t) + \mathbf{e}(t) \quad (2.26)$$

the noise source  $\mathbf{e}(t)$  is white and the matrix  $K$  plays a role to determine the spectrum of the noise. Now consider again expression 2.12. to explicitly specify a system model  $G(z)$  and a noise model  $H(z)$ . They are related to the system matrices according to

$$G(z) = C(zI - A)^{-1}B + D \quad (2.27)$$

and

$$H(z) = C(zI - A)^{-1}K + I \quad (2.28)$$

For the subspace identification we would like to estimate the system matrices ( $A$ ) from measured input and output data. If also the states were also known, then the solution would be straightforward: Compute  $C$  and  $D$  with linear regression, reconstruct  $\mathbf{e}(t)$ , compute  $A$ ,  $B$  and  $K$  also with linear regression. The subspace identification is used to find the states. An important aspect of this problem is to

determine the number of states, so the order  $n$  of the system. Now an essential step is the reconstruction of the (extended) observability matrix:

$$\mathcal{O} = \begin{bmatrix} C \\ CA \\ CA^2 \\ \vdots \\ CA^{n-1} \end{bmatrix} \quad (2.29)$$

from input-output data which can be performed by least-square like (projection) steps. The rank of this matrix equals the order  $n$  of the system and Singular Value Decomposition can be applied for this purpose (28). Once the rank and the observability matrix are known, it is easy to determine  $C$  and  $A$ . Output matrix  $C$  equals the top part of this matrix and this result can be used to compute  $A$  from the rest. Furthermore, the states and the noise contributions can be estimated. The matrices  $B$  and  $D$  as well as the initial states are estimated from a linear regression problem. An overview of subspace techniques is given by Ljung (27) and Katayama (28).

#### 2.4.3.1. Comparison Prediction Error and Subspace method

Nowadays both subspace (N4SID in matlab) and prediction error (PEM in matlab) are available in the numerical computing software packages. In general, iterative prediction error algorithms give better results. However, the subspace method well suited as an initial guess to obtain better prediction error models (29) (28).

The PEM algorithm in 'MATLAB' also benefits from this features when no initial parameter values are given.

A summary of (dis)advantages of both strategies are briefly described in the list below.

- The applied model structure of a state space system has no need for a more explicit definition of the model equations. Only the model order of the system matrix should be selected.
- Subspace method is well suited for MIMO
- Numerical and mathematical approach of the subspace method is elegant (robust, reliable) and efficient (optimization with linear equations).
- The subspace method is non iterative
- Not all mathematical issues of the optimization in subspace algorithms are settled
- The obtained solution of the subspace method is "sub-optimal"

### 2.4.4. Recursive identification

During movement, linear perturbation and modeling techniques will fail because the system states transit continuously through different points of operation leading to nonlinear behavior. In addition, the properties may also be time-variant. This implies that for movement analysis, a time-varying approach is required to identify the neuromuscular properties.

In addition load dynamics can vary in time. This also requires a time dependent model estimation algorithm. For example consider a second order system whose dynamics can be characterized by means of a second order transfer function. While exciting the system with a proper disturbance signal  $x(t)$ , the system's output signal  $y(t)$  is recorded. At  $t = t_a$  the dynamics of the system suddenly changes. This can be mathematically described as:

$$H(s) = \frac{X(s)}{F(s)} = \begin{cases} 1/(M_1s^2 + B_1s + K_1) & t \leq t_a \\ 1/(M_2s^2 + B_2s + K_2) & t > t_a \end{cases}$$

For convenience we use force  $F(s)$  as input and position  $X(s)$  as output. Furthermore the physical parameters are mass, damping and stiffness labeled with  $M$ ,  $B$  and  $K$  respectively. Objective is to track the parameter values in time. Therefore we will choose a recursive parametric identification tool which will be outlined in the following sections.

#### 2.4.4.1. Recursive algorithm

Suppose that the least squares criterion in equation 2.17 is extended by a weighting function  $\beta(t, k)$ :

$$V_t(\theta) = \sum_{k=1}^t \beta(t, k) [y(k) - \varphi^T(k)\theta]^2 \quad (2.30)$$

which has the following properties:

$$\beta(t, k) = \lambda(t)\beta(t-1, k), \quad 0 \leq k \leq t-1 \quad (2.31)$$

$$\beta(t, t) = 1 \quad (2.32)$$

This implies:

$$R(t) = \lambda(t)R(t-1) + \varphi(t)\varphi^T(t) \quad (2.33)$$

$$f(t) = \lambda(t)f(t-1) + \varphi(t)y(t) \quad (2.34)$$

One can calculate the estimated parameter vector:

$$\begin{aligned} \hat{\theta}_t &= R^{-1}(t)f(t) \\ &= R^{-1}(t) [\lambda(t)f(t-1) + \varphi(t)y(t)] \\ &= R^{-1}(t) [\lambda(t)R(t-1)\hat{\theta}_{t-1} + \varphi(t)y(t)] \\ &= R^{-1}(t) [R(t) - \varphi(t)\varphi^T(t)] \hat{\theta}_{t-1} + \varphi(t)y(t) \\ &= \hat{\theta}_{t-1} + R^{-1}(t)\varphi(t) [y(t) - \varphi^T(t)\hat{\theta}_{t-1}] \end{aligned} \quad (2.35)$$

With equations 2.34 and 2.35 we now have a recursive algorithm, which complies with the requirement that the current estimate of the parameter vector is calculated using information already accumulated from previous measurements. At time  $t - 1$  only the finite-dimensional information vector is stored:  $X(t - 1) = [\hat{\theta}(t - 1), R(t - 1)]$ , at time  $t$  this vector is updated using 2.35.

By introducing  $P(t) = R^{-1}(t)$  and using the matrix inversion lemma:

$$[A + BCD]^{-1} = A^{-1} - A^{-1}B[DA^{-1}B + C^{-1}]^{-1}DA^{-1} \quad (2.36)$$

the Recursive Least Squares Algorithm (RLS) can be summarized by the well known expressions:

$$\hat{\theta}(t) = \hat{\theta}(t - 1) + L(t)[y(t) - \varphi^T(t)\hat{\theta}(t - 1)] \quad (2.37)$$

$$L(t) = \frac{P(t - 1)\varphi(t)}{\lambda(t) + \varphi^T(t)P(t - 1)\varphi(t)} \quad (2.38)$$

$$P(t) = \frac{1}{\lambda(t)} \left[ P(t - 1) - \frac{P(t - 1)\varphi(t)\varphi^T(t)P(t - 1)}{\lambda(t) + \varphi^T(t)P(t - 1)\varphi(t)} \right] \quad (2.39)$$

$$\hat{\theta}(0) = \text{arbitrary}$$

$$P(0) = \text{positive definite matrix}$$

**Forgetting Factor Approach** By assigning less weight to older measurements that are not representative for the system in the weighted criterion 2.18 system variations will be tracked in a natural way. When choosing  $\lambda(j) < 1$ , in particular  $\lambda(j) \equiv \lambda$ , then in terms of 2.32:

$$\beta(t, k) = \lambda^{t-k} \quad (2.40)$$

and old measurements will be exponentially discounted. In section B.2 of Appendix B, an alternative method is described to distinct the contribution of current and older measurements.

## 2.5. Non parametric identification

Non parametric models use description that make no assumptions about system structure or order and are infinite dimensional in nature. Consequently, they are well adapted to the study of unknown systems.

### 2.5.1. Frequency response models

The most common linear nonparametric model used to describe dynamics is the linear frequency response model. The relation between position and force can be described by a compliance frequency response function (FRF):

$$X(\omega) = P(\omega)F(\omega) \quad (2.41)$$

Where position  $X(\omega)$ , Force  $F(\omega)$  and compliance  $P(\omega)$  are Fourier transformed.

Because direct transformation is often impossible a, spectral estimator of the system is given by:

$$H_{uy}(\omega) = \frac{\Theta_{uy}(\omega)}{\Theta_{uu}(\omega)} \quad (2.42)$$

Where  $\Theta_{uy}(\omega)$  is the cross spectral density (CSD) of  $u$  and  $y$ , and  $\Theta_{uu}(\omega)$  is the power spectral density (PSD) of the input  $u$ . The PSD of  $u$  can be expressed as:

$$\Theta_{uu}(\omega) = E[u(-(\omega)u^T(w))] \quad (2.43)$$

And the CSD of  $u$  and  $y$  as:

$$\Theta_{uy}(\omega) = E[u(-(\omega)y^T(w))] \quad (2.44)$$

Estimation of human arm dynamics in frequency domain has been performed by van der Helm et al.(4). Note that in this particular case, identification was performed under closed loop conditions.

### 2.5.2. Impulse response models

In the time domain, models may be formulated as impulse response functions (IRF).

$$x(t) = \int_0^{\infty} p(\tau)F(t - \tau)d\tau \quad (2.45)$$

The IRF is simply the inverse Fourier transforms of equation (2.41) and does not provide any additional information in principle. However, the two approaches provide complementary insights of the system behavior, and moreover the estimation techniques display different performance.

Estimation of human dynamics in time domain has been performed by Kearney et al. (5).

### 2.5.3. Closed loop identification

As being suggested in the introduction, certain interaction classes result in a closed loop configuration of the human (e.g. human arm) and load. In figure 2.5 the general situation of two system operating in closed loop is depicted.

Closed-loop system identification leads to several difficulties due to the correlation between the disturbances and the control signal induced by the loop. According to (27) and (30) three approaches are suitable to identify a system operating in closed loop. We will discuss them briefly.

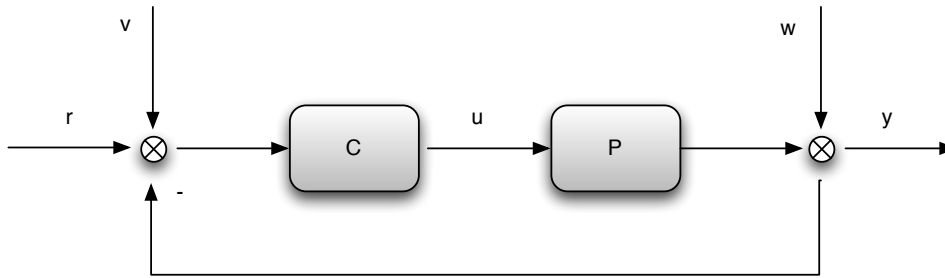


**Figure 2.5.:** Closed loop system, with plant P and controller C. The signals are labeled as  $r$  = reference,  $u$  = input,  $y$  = output,  $v$  = system noise,  $w$  = measurement noise

#### 2.5.3.1. Direct approach

Applying the direct approach in closed loop system results in an estimate of the frequency response function (FRF) that contains both the dynamics of the controller (C) and plant (P). The contribution of both parts to the total FRF depends on the system and measurement noise ratios. When both noise sources are unknown it is impossible to distinguish C and P in the estimated FRF. This can be illustrated by the transfer from  $u$  to  $y$ :

$$H_{uy}(\omega) = \left( \frac{\Theta_{ww}(\omega)}{\Theta_{vv}(\omega) + \Theta_{ww}(\omega)} \right) \frac{-1}{C^T(\omega)} + \left( \frac{\Theta_{vv}(\omega)}{\Theta_{vv}(\omega) + \Theta_{ww}(\omega)} \right) P^T(\omega) \quad (2.46)$$

Where  $\Theta_{ww}$  and  $\Theta_{vv}$  are power spectral densities of respectively  $v$  and  $w$ , see figure 2.5. The transfer function shows that when a passive linear stationary load is considered as a plant being controller by the human, direct approach will result in an estimation of the plant dynamics because  $\Theta_{ww}$  will be significant lower than  $\Theta_{vv}$  (31).

#### 2.5.3.2. Indirect approach

The indirect approach is an extension of the direct approach with in difference that either prior plant or controller dynamics are known. Unknown dynamics of either plant or controller can now be fully derived.

### 2.5.3.3. Joint input-output approach

The joint input-output approach uses prior knowledge of the disturbance signal  $v$  or  $w$  (see figure 2.5). Hence known perturbations have to be applied to the closed loop system.

Dividing the cross-spectral-density between  $w$  and  $y$  identifies the controller dynamics:

$$\frac{\Theta_{ww}(\omega)}{\Theta_{wy}(\omega)} = \frac{-\Theta_{ww}(\omega)M^T(\omega)}{\Theta_{ww}(\omega)S^T(\omega)} \quad (2.47)$$

with  $S^T$  the sensitivity of the system output to disturbances  $w$ , which is defined as:

$$S^T(\omega) = \frac{\Theta_{wy}(\omega)}{\Theta_{ww}(\omega)}; \quad (2.48)$$

where  $\Theta_{wy}$  is the cross spectral density of the output  $y$  and noise term  $w$ . This finally results in:

$$\frac{\Theta_{ww}(\omega)}{\Theta_{wy}(\omega)} = -\frac{S^T(\omega)C^T(\omega)}{S^T(\omega)} = -C^T(\omega) \quad (2.49)$$

A similar derivation is possible for the description of plant dynamics.

### 2.5.4. Identification of physiological meaningful parameters

Dynamic systems in the physical world are naturally described in continuous time (CT), differential equation terms because the physical laws, such as conservation equations, have been evolved mainly in this form. Paradoxically, however, the majority of known system identification schemes have been based on discrete-time (DT) models, without much concern for the merits of natural continuous-time model descriptions and their associated identification methods. In fact, the development of CT system identification techniques occurred in the the last century, before the development of the DT techniques, but was overshadowed by the more extensive DT developments (32).

A consequence of demanding physiological meaningful parameters, like stiffness, damping and inertia, is that discrete-time model descriptions have to be converted to their continuous time equivalents.

#### 2.5.4.1. Discrete to continuous domain conversion

When physical insight of a dynamic system is required only parameters in the continuous domain are relevant. We should therefore convert parameter estimations in the discrete domain to the continuous domain, or Laplace to Z domain.

The bilinear transform or Tustin transformation is a first-order approximation of the natural logarithm function that exactly maps the  $z$ -plane to the  $s$ -plane. Moreover it maps the left half  $s$ -plane to the unit circle of the  $z$ -plane. Hence systems designed in the continuous domain preserve stability after conversion.

The inverse bilinear transformation can be described by:

$$\begin{aligned}
 s &= \frac{1}{T} \ln(z) & (2.50) \\
 &= \frac{2}{T} \left[ \frac{z-1}{z+1} + \frac{1}{3} \left( \frac{z-1}{z+1} \right)^3 + \frac{1}{5} \left( \frac{z-1}{z+1} \right)^5 + \dots \right] \\
 &\approx \frac{2}{T} \frac{z-1}{z+1} \\
 &\approx \frac{2}{T} \frac{1-z^{-1}}{1+z^{-1}}
 \end{aligned}$$

Where,  $s$  is the Laplace variable,  $T$  the sampling interval and  $z$  is the shift operator in the  $z$  domain.

Transform of the well known second order equation:

$$H(s) = \frac{X(s)}{F(s)} = \frac{1}{Ms^2 + Bs + K} \quad (2.51)$$

gives:

$$H(z) = \frac{X(z)}{F(z)} = \frac{1 + 2z^{-1} + 2z^{-2}}{\left(\frac{4M}{T^2} + \frac{2B}{T} + K\right) + \left(\frac{-8M}{T^2} + 2K\right)z^{-1} + \left(\frac{4M}{T^2} - \frac{2B}{T} + K\right)z^{-2}} \quad (2.52)$$

Mapping from discrete to continuous domain is now possible using:

Using:

$$H(z) = \frac{X(z)}{F(z)} = \frac{b_0 + b_1z^{-1} + b_2z^{-2}}{a_0 + a_1z^{-1} + a_2z^{-2}} \quad (2.53)$$

We can map the discrete parameters,  $a_0 \dots a_2$ , to the continuous mass, damping, spring values by:

$$\begin{bmatrix} a_0 \\ a_1 \\ a_2 \end{bmatrix} = \begin{bmatrix} 4/T^2 & 2/T & 1 \\ -8/T^2 & 0 & 2 \\ 4/T & -2/T & 1 \end{bmatrix} \begin{bmatrix} M \\ B \\ K \end{bmatrix} \quad (2.54)$$

$$\hat{\theta}_d = A\hat{\theta}_c \quad (2.55)$$

Using matrix inversion we can calculate the estimated continuous parameter values  $\theta_c$ .

### 2.5.5. Model Validation

The parameter estimation procedure picks the best model within the chosen model structure. Now the question is whether this model is good enough. Important aspects within this research includes the question if the estimated model describes the true system. An indication of the goodness of model fits, the variance accounted for (VAF) scores can be calculated:

$$\text{VAF} = 1 - \frac{\sum_{i=1}^N |y(t_i) - \hat{y}(t_i)|}{\sum_{i=1}^N |y(t_i)|^2} \quad (2.56)$$

Next important source to validate the model follows from analysis of residuals:

$$\epsilon(t, \hat{\theta}_N) = y(t) - \hat{y}(t|\hat{\theta}_N) \quad (2.57)$$

First importance is that the residuals do not depend on the input. To check this it is reasonable to study the covariance between residuals and past inputs:

$$R_{\epsilon u}(\tau) = \frac{1}{N} \sum_t^N = \epsilon(t)u(t - \tau) \quad (2.58)$$

In an ideal situation cross correlation would result in a white gaussian signal.

When traces of past inputs are visible in the residuals, then there is a part of  $y(t)$  that originates from the past input and that has not been properly picked up by de model. If correlation is found for negative lags ( $\tau < 0$ ) than output has been fed back to the input. This also indicates if measurements are taken in closed loop situation.

When correlation among the residuals themselves is found, i.e.

$$R_{\epsilon\epsilon}(\tau) = \frac{1}{N} \sum_t^N = \epsilon(t)\epsilon(t - \tau) \quad (2.59)$$

are not small for  $\tau \neq 0$ , then part of  $\epsilon(t)$  could have been predicted from past data. This means that  $y(t)$  could have been better predicted.

## 2.6. Conclusions of discussed identification algorithms

Because we're primary interested in the physical load parameters, only parametric identification methods are considered. Table 2.1 gives an overview of discussed identification algorithms together with their dis(advantages). All four methods have been used to estimate load dynamics.

Name	Advantages	Disadvantages
ARX	unique least squares solution which can be solved analytical	fixed disturbance model structure
PEM	variety of system and disturbance structures	iterative search in parameter space, local minimum possible
Subspace	non iterative, fast, robust, suitable for MIMO	can result in suboptimal solutions
Recursive ARX	allows varying parameter values	slow convergence to real parameter values

**Table 2.1.:** Summary of proposed system identification algorithms



## 3. Methods

This chapter will discuss how different research questions, as stated in the introduction, can be answered and how identification and tasks evaluation objectives will be fulfilled. In order to validate theories obtained from previous research studies, which have been summarized in the previous chapter, and subsequently apply them in new algorithms, an experimental setup has been developed. In addition, a number of model studies has been conducted. These preliminary model studies are used either for demonstrating the essence of different algorithms or as a preliminary investigation of a particular experimental condition. In order to provide a clear story line of this thesis, model studies are not embedded.

This chapter will start by describing three different arm tasks which will be used as task instructions in the experimental setup. Then an introduction of the experimental setup will be given and the measurement protocol and analysis of acquired data will be discussed.

In addition, measurements obtained from a preceding experimental study, where similar interface sensors have been used, have been evaluated using the same identification algorithms. The methods of this experimental study have been outlined in the final section of this chapter.

### 3.1. Daily life tasks

Three different arm tasks are proposed. They provide both coordinate constrained tasks and tasks where the essence relies on maximization of applied forces and generated arm velocities.

Next subsections will describe the tasks successively. After a basal description, the task instruction and a number of sport activities which are related to the task are given. Furthermore a few keywords are given which characterize each task in physical terms. Subsection 3.1.6 describes a model extraction for every functional task. Finally an indication of imposed disturbances is given while performing the suggested tasks.

#### 3.1.1. Displace object: Minimal duration

The subject is asked to accurately displace an object in a minimum amount of time. The object to be manipulated is mainly characterized by a mass load. Accurate is defined as a minimal deviation between target and movement endpoint position.

This task is comparable to an abundance of tasks, like displacing an object or any other manipulation of daily used objects. Visual feedback plays an important role in these tasks.

### 3.1.2. Throw object: Maximal momentum

The subject is asked to throw an object as far as possible. This involves a maximal torque generation around the elbow joint just before releasing the object. We only consider the elbow joint because performed movements are restricted to be planar in the transverse body plane. The object to be thrown is considered to be a point mass. The load release causes a force disturbance and is effectively exciting the human body. Hence body responses will be available at interface sensors.

This task is comparable with activities like throwing a ball, playing darts or shuffleboard. Forces are predominantly generated by biceps and triceps muscles.

### 3.1.3. Punch object: Maximal momentum

The subject is asked to punch into an obstacle with maximal momentum. This obstacle can be considered as a highly viscous medium. The user's hand is equipped with a mass load. Again when impact occurs disturbance forces will be felt by the user. This leads to reaction forces visible at the contact interface.

Comparable activities to this simplified task in sports are boxing and some other martial arts, but also swimming has commonalities.

### 3.1.4. Task summary

The following table gives an overview of proposed daily life tasks. The first column give the different tasks as discussed in this section. Second column gives the task objective and final column shows the boundary conditions when applied.

Experimental setup name	Task objective	Boundary condition
Displacing Object (DO)	Min. Time	Min. Endpoint accuracy
Throwing Object (TO)	Max. Impuls	-
Punching Object (PO)	Max. Impuls	-

**Table 3.1.:** Summary of proposed daily life tasks.

### 3.1.5. Identification requirements

The usability of measured forces and movement signals for the identification process depends on the quality of excitation signal. Additionally non linearities of the system imposes the (linear) identification process to operate in a quasi linear working point. Furthermore a non-stationary system will guarantee the validity of the identification

process only in certain time frames where the system can be considered as stationary. Duration and power content of frequencies where the load dominates, strongly influences identification results.

### 3.1.6. Load disturbances

Event transitions in the described tasks, e.g. the release of the object cause disturbances in either the human body or load. These disturbances lead to responses of the dynamic systems involved. Prior knowledge about start of the disturbance will therefore be necessary to give a causal explanation of the response.

In table 3.2 disturbance characteristics are given for all tasks.

	Source	Onset	Magnitude
Displace Object	$F_{ext}$	continuous	max 70 N
Throw Object	$\downarrow m_l$	$< 1 s$	3-23 kg
Punch Object	$\uparrow b_l$	$< 1 s$	290 Nm/s

**Table 3.2.:** Disturbance characterization of different tasks:  $m_l$  = load mass,  $b_l$  = load viscosity,  $F_{ext}$  = external force source. First column is the task name, second and third gives the cause and start of disturbance, and last column indicates the magnitude of this change in dynamics. During the first task type ('displace object'), no disturbance will be induced by change in object dynamics. The only active force source is generated by the biceps/triceps muscles.

## 3.2. Experimental setup

### 3.2.1. Comparison of appropriate setups

An essential requirement of the experimental setup is the ability to measure kinematic and kinetic quantities on the interface of human body and load. In this research work we will merely focus on tasks where arm and hand are involved. This implies that force sensors should be as close as possible to the pressure spot(s) of the subject's hand.

Different experimental setups have been considered and evaluated (see table 3.2 for a comparison). In addition a comparison with physical loads is given. Aspects regarding flexibility (variety of loads which can be simulated), range (max. and min. load parameter values), sensitivity (minimal change in output movement to input forces), accuracy (accuracy of rendered movement) and complexity (how to obtain force and movement information) are summed up. As can be seen in the mentioned table, both 'HapticMASTER' and 'Wristalizer' from Moog (33) allow a wide variation of load configurations. It furthermore shows acceptable properties within perspective of this research work. Therefore, the 'HapticMASTER' (see figure 3.1), was chosen as the instrument for the experimental studies.

	Control type	Flexibility	Range	Sensitivity	Accuracy	Complexity
Physical loads	-	- -	++	++	++	-
HapticMASTER (33)	Admittance	++	+	+	+	+
Wristalizer (33)	Admittance	+	$\pm$	+	+	+
Phantom (34)	Impedance	+	-	++	+	+

**Table 3.3.:** Weighted criteria for suitable experimental setup.

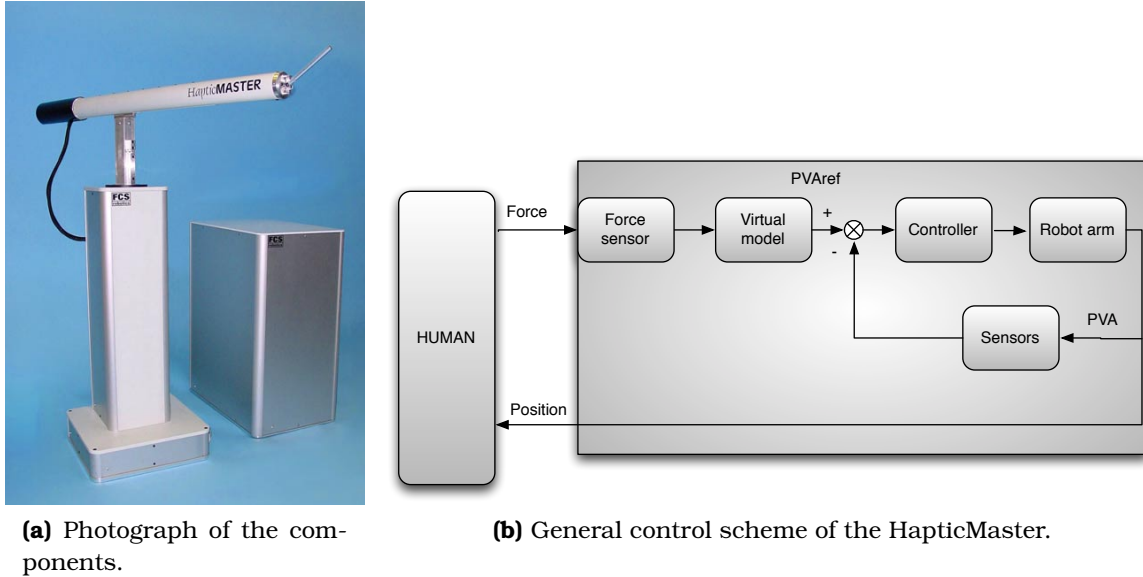


**Figure 3.1.:** Moog's 'HapticMASTER'. On the left the haptic robot arm and on the right the control unit. On the right the control diagram, comprising an outer control loop, and an inner servo loop. A (virtual) model converts the force sensor signal to a Position/Velocity and Acceleration (PVA) set-point vector. The inner servo loop controls the robot to the PVA set-point values. Adapted from (35).

### 3.2.2. HapticMASTER

The 'HapticMASTER' is a three degrees of freedom, force-controlled haptic interface. The programmable robot arm utilizes the admittance control paradigm, giving the device unique specifications. It provides the user with a natural haptic sensation and the power to closely simulate the weight and force found in a wide variety of tasks.

The hardware of the hapticmaster comprises two functional components: the robot arm and a control unit (see figure 3.1a). A sensitive strain gauge force sensor is located right after the end effector at the end of the robot arm. The interaction force is measured as close to the human hand as possible, to avoid distortion of the force signal and to optimize system performance.

Communication with the control unit is possible using the application programming interface (API). The API functions are written in C++ language and therefore suitable for multiple platforms.

For a complete specification list see table A.1 which is located in the appendix A.

### 3.2.3. Additional devices.

**Xsens MT9** As the hapticmaster does not register accelerations, an additional 3D Inertial Measurement Unit (IMU) from Xsens Technologies (MT9) was mounted. This IMU is equipped with accelerometers, rate-gyroscopes and magneto sensors and is able to accurately estimate the kinematics with respect to the global world frame. The inertial sensor is capable of measuring accelerations ranging from  $-100 \text{ m/s}^2$  to  $100 \text{ m/s}^2$ . This should be sufficient for most explosive arm sports (36) and therefore suitable for all mentioned arm tasks.

## 3.3. Experimental protocol

In figure 3.2, the environment, in which the subject is performing different tasks along with the hapticmaster is depicted. A lateral projection shows different stage parts and gives an overview of how the subject is positioned. In addition, in figure 3.3 a subject is depicted who is performing a task in the actual 'virtual' environment.

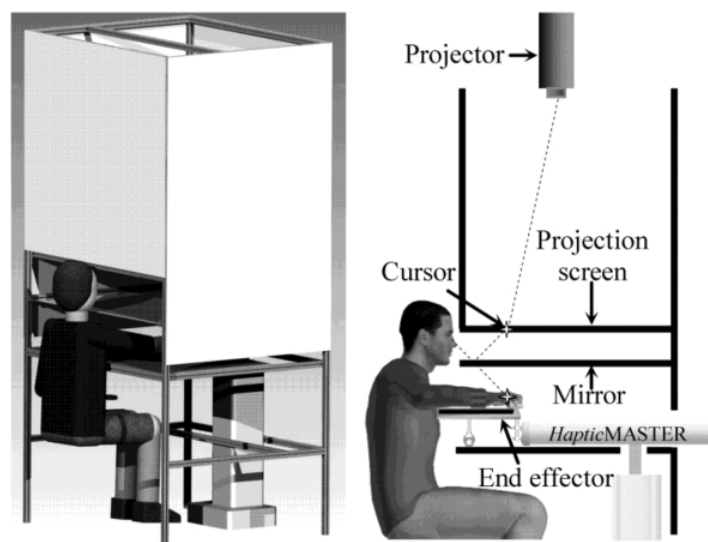


**Figure 3.2.:** Illustration of the hapticmaster setup. On the left a scaffold with integrated projection screen and hapticmaster robot. On the right a lateral projection of the total setup.

The virtual environment can be divided in a haptic and a visual environment. Haptics are rendered by the hapticmaster's controller and will be encountered by the subject when his/her hand firmly holds the end effector knob. The visual part manifests to the subject using a beamer which is projecting on a mirror. There is a real time connection between both environments which allow realtime visual presentation of embedded haptic model parts. The visuals are generated using the OpenGL platform and programmed in C++ language such that it is embedded with other necessary control and measurement software.



(a) Subject performing a task.



(b) Working area of the environment.

**Figure 3.3.:** Subject positioned in hapticmaster environment while performing an instructed arm task. On the right the working area of the hapticmaster environment is depicted. Movements are restricted to the transverse plane. On top the mirror on which a visual environment is projected. In front of the mirror is a black piece of particleboard mounted to inhibit direct vision of the arm. The IMU is hardly visible, though the signal output is (black connector/grey cable).

A thin mirror and black piece of particleboard inhibits direct vision of the subject on the subject's arm. This allows us to manipulate visual feedback when demanded.

Different interaction situations will be simulated using the HapticMASTER. One can program almost any virtual environment which consists of objects with specified dynamic properties. Subsequently running the virtual environment on the target computer allows realtime rendering of haptics and visuals.

### 3.3.1. Protocol

Eight subjects, with ages from 21 to 27 years, all right-handed and no known neuromuscular anomalies, were recruited on a voluntary basis. The test subject gave informed consent to participate in the study. The test subject was seated comfortably in front of the virtual environment. The seat was adjusted so that he/she had a good view of the virtual environment (see figure 3.3). Only planar movements in the transverse plane were allowed. Figure 3.4 shows the working area of the HapticMASTER and specific points of interest.

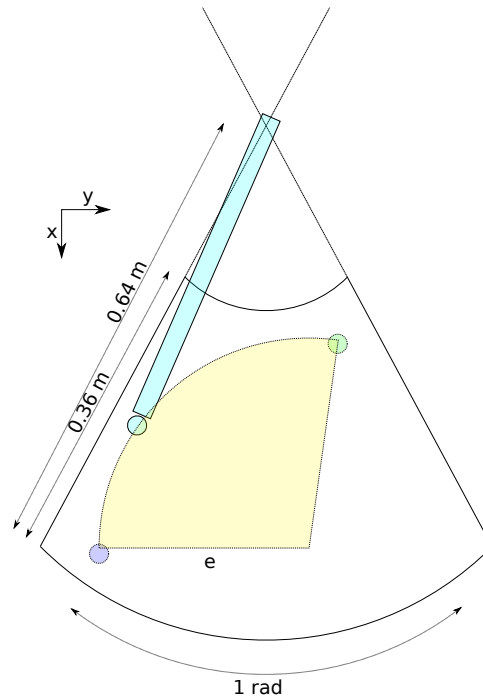


**Figure 3.4.:** Working area of the HapticMASTER. Actual dimensions are given,  $e$  is the length from elbow to the center of the subject's hand. Blue indicates the robot arm, whereas the dot indicates the end-effector. The purple and the green dot indicate begin and endpoint positions for the displacement task. The disc piece illustrates the total elbow flexion/extension. Finally the red area indicates deviations of the position.

The subject was asked to hold the black knob of the hapticmaster with his/her right hand. In case of unpredicted behavior of the HapticMASTER, a red stop button is approachable by the subject's left hand.

Table 3.2 gives a brief overview of disturbances being experienced by the subject while performing one of the three tasks. The subject was asked to perform three different tasks. Every task was divided in four blocks (5, 10, 15 and 25 kg) of 10 trials, giving a total of 40 trials. Every block of trials was performed with a different simulated endeffector inertia. The order of the second, third and fourth block of trials with equal inertia was randomly selected. All three tasks were repeated once, resulting in 240 trials per subject.

Table 3.4 describes the task instructions for each task in order as performed by the different subjects. Figures 3.5 show the different visual environments as shown to the subjects. Furthermore specific task related requirements are listed. A maximum force  $F_{max}$  appliance to the end effector of 70 N is prescribed as a general requirement.

	Task Goal	Boundary Condition(s)
Displace Object (fig. 3.5a)	$\min(t_b - t_a)$	<sup>a</sup> and $\ x(t) - x_e\  < \epsilon, \forall t > t_{c1}$ <sup>b</sup>
Throw Object (fig. 3.5b)	$\max(p(t_{b,circum}))$	<sup>a</sup>
Punch Object (fig. 3.5c)	$\max(p(t_{b,circum}))$	<sup>a</sup>

<sup>a</sup> General restriction:  $\|F\| < \|F_{max}\|$

<sup>b</sup>  $x(t)$  = end effector position,  $x_e$  circle center position,  $\epsilon$  radius of circle,  $t_{c1}$  time at first collision with circle circumference.

**Table 3.4.:** Task instructions. See figure 3.5 for corresponding task interface layout.

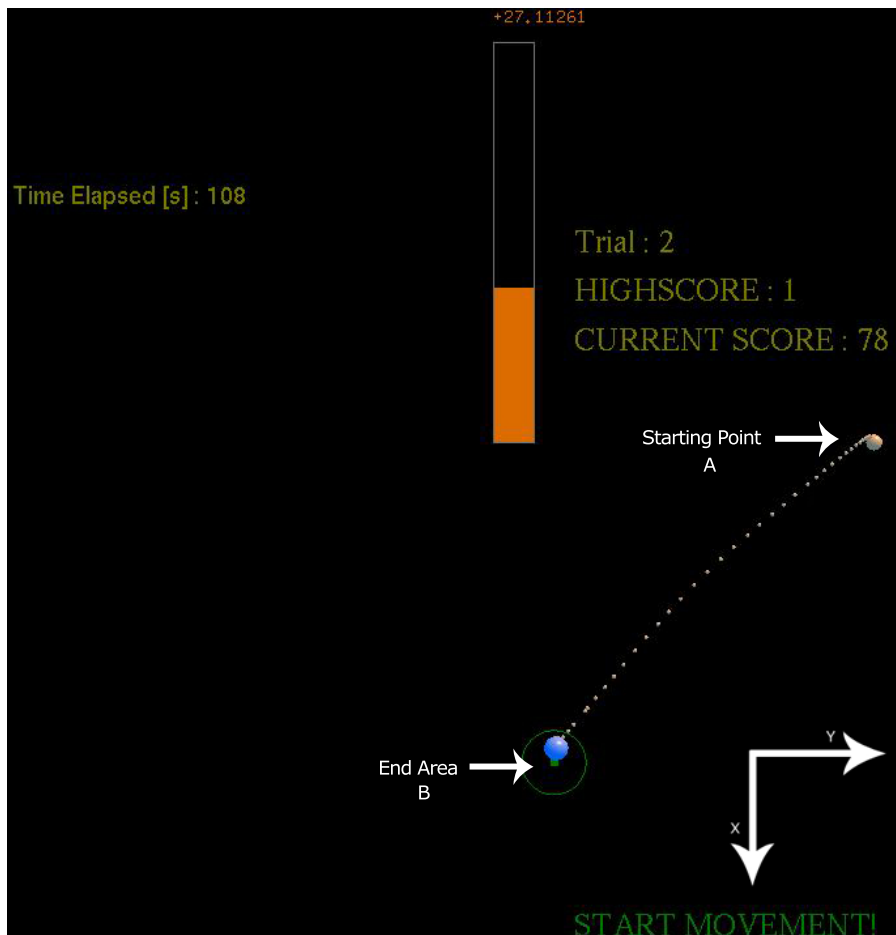
### 3.3.2. Signal Processing

Forces, velocities and positions of the end effector are obtained by readout recordings of the HapticMASTER's status. As the HapticMaster does not offer an instantaneous output, polling of its status is required. Hence reconstruction of the signal time base is necessary.

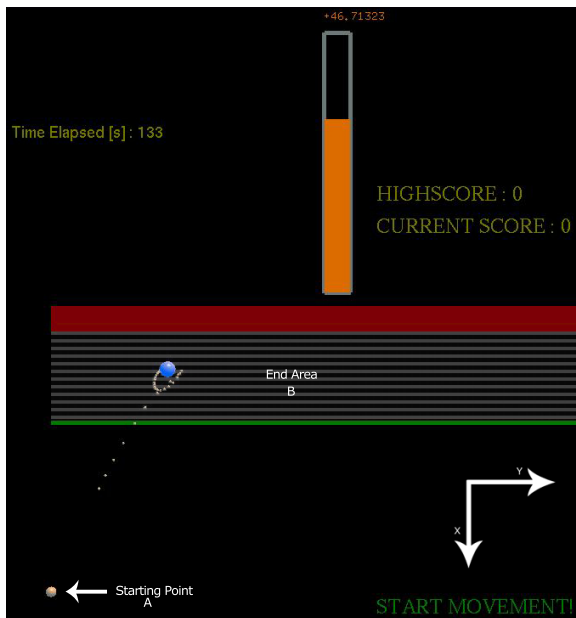
#### 3.3.2.1. Force en movement signals

Force and movements signals are gathered by the interface software and written in plain text to the hard-drive. Next MATLAB is used to process all signals. In the following list all processing steps are given in sequential order.

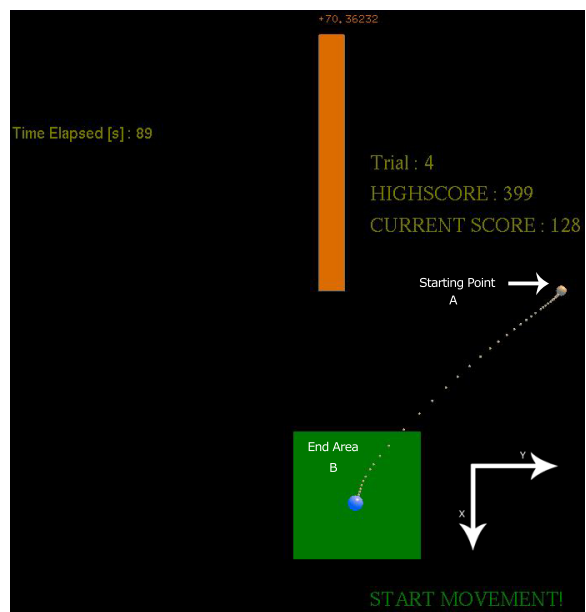
- Join interrupted data sequences. Interruptions are caused by the subject who exceeds haptimaster's safety margins.
- Create a uniform sampled dataset and resampling at 400 Hz. The resample frequency of 400 Hz is determined by the average polling interval.
- Differentiate Hapticmaster's velocity for an estimation of the accelerations.
- Low pass filtering using 5th order buttorworth filter with a cutoff frequency of 5 Hz. Forward and backwards filtering to avoid phase delays.
- Estimate initial orientation of the Xsens module using a zero velocity interval of 1 s and knowledge of sensor frame axes.
- Align frames of the hapticmaster and Xsens module, see 3.3.2.2.
- Shift of accelerometer signals, explanation can be found in experimental evaluation chapter.
- Collision detection based upon negative accelerations.
- Check if the trials meet the boundary conditions as stated in table 3.4.



(a) Displace Object



(b) Throw Object



(c) Punch Object

**Figure 3.5.:** Task interfaces as shown to the subjects. On top of the interface, a bar is shown which displays the maximum force applied to the end effector during one trial. On the right hand side of the bar, three lines display the trial number, maximum score obtained in one block of ten trials and the score of the last trial respectively. When the subject did not fulfill the boundary condition, the current score will be displayed in red and does not count towards the high score.

- Evaluate the performance of the subject during trials, see section 3.3.2.3.
- Estimate the parameters of the simulated dynamics, see section 3.3.2.4.

### 3.3.2.2. Frame alignment

Signal operations where both movement and force sensors are involved, require an alignment of both reference frames. When the end effector of the hapticmaster is displaced, the Xsens' sensor frame will be displaced with respect to the hapticmaster reference frame.

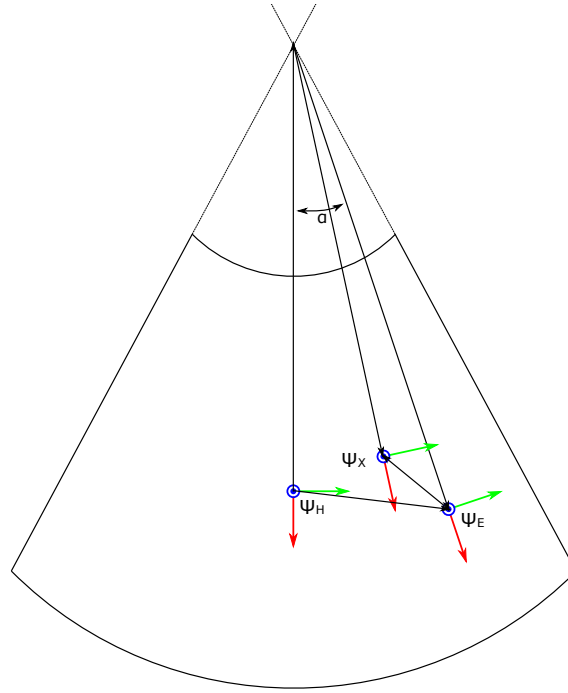


**Figure 3.6.:** Coordinate frames of respectively the Hapticmaster, ( $\Psi_H$ ), End-effector ( $\Psi_E$ ) and Xsens ( $\Psi_X$ )

In order to align both frames we should estimate the orientation and position of the endeffector frame ( $\Psi_E$ ) with respect to the hapticmaster frame ( $\Psi_H$ ) as showed in the following equation:

$$\begin{bmatrix} \mathbf{p}^H \\ 1 \end{bmatrix} = \begin{bmatrix} R_E^H & \mathbf{p}_E^H \\ \mathbf{0}_3^T & 1 \end{bmatrix} \begin{bmatrix} \mathbf{p}^E \\ 1 \end{bmatrix} \quad (3.1)$$

The position and orientation of the Xsens sensor with respect to the end effector frame  $\Psi_E$  remains constant during the movement and is expressed as  $\mathbf{p}^E$ . Now  $\mathbf{p}^H$  is the position of Xsens frame  $\Psi_X$  expressed in the hapticmaster frame  $\Psi_H$ . This can be calculated using a homogenous transformation matrix. This matrix includes a rotation matrix  $R_E^H$  describing the orientation of the end effector frame  $\Psi_E$  expressed in  $\Psi_H$ . It furthermore includes the vector  $\mathbf{p}_E^H$  which described the translation of frame  $\Psi_E$  to  $\Psi_H$ . This vector is obtained directly by the positional output of the hapticmaster.

The rotation matrix is obtained by prior knowledge of the end effector arm length and the angle between  $\Psi_H$  and  $\Psi_E$  which is denoted as  $\alpha$ . Parametrization by a single angle is sufficient, because only planar movements are considered.

After  $\mathbf{p}^H$  is calculated we can finally construct the rotation matrix  $R_X^H$  to express accelerations of the Xsens sensor in the hapticmaster frame.

$$\mathbf{a}^H = R_X^H \mathbf{a}^X \quad (3.2)$$

### 3.3.2.3. Evaluation of task performance

The subject's task performance has been evaluated when he/she stops moving and the software indicates the end of a movement. The subject's score was notified by a number which has been calculated using the equation described in the second column of table 3.4, which is respectively the movement duration (first task) and applied impulse (second and third task). For the object displacement task, the inverse is taken such that for all tasks the objective to score as high as possible.

These are just examples of how performance of the user could be judged using interface sensing. Hence, other tasks, for example endurance tasks, may have other task demands.

### 3.3.2.4. Identification of simulated dynamics

Four system identification algorithms were applied to the measured interface forces / acceleration / velocities and positions. First is the 'linear in parameters' ARX method, second the subspace method called n4sid, third is the iterative prediction error method (PEM) and finally a recursive identification method has been used. All algorithms have been described in the background chapter. An summary of specific Furthermore, the non iterative sub-space method has been used to indicate an optimal model order.

Data sets of the second and third task (Throw Object/ Punch Object) have been split at the onset of change in system dynamics. Identified models were analyzed using the force input signals. The movement and parameter output has been compared to the actual measured output and known simulated parameters which allows us to give an error analysis of identified loads.

### 3.4. Physical load experiments

The system identification algorithms were furthermore applied to physical load experiments. These experiments were performed in a former study where power exchange between human and load was evaluated using force and inertial interface sensors (37). Task performance was not evaluated during these experiments.

Kinematic and kinetic quantities were measured in the handle between the hand and the load. 3D forces and moments were measured using a 6 DOF force/moment sensor module. 3D movement was measured using 3D accelerometers and angular velocity sensors.

A 3D accelerometer senses the difference between inertial ( $\mathbf{a}$ ) and gravitational ( $\mathbf{g}$ ) acceleration:

$$\mathbf{s}_a = \mathbf{a} - \mathbf{g} \quad (3.3)$$

Now, inertial acceleration can be estimated from accelerometer signals by adding the gravitational acceleration  $\mathbf{g}$ . Since  $\mathbf{g}$  is directed vertically and has a constant known norm ( $\approx 9.81$ ) addition is possible when the orientation of the accelerometer sensor frame with respect to the global frame is known.

Orientation can be obtained by solving the following differential equation:

$$\dot{\mathbf{R}}_s^g = \mathbf{R}_s^g \tilde{\omega}_{s,g}^s \quad (3.4)$$

Where  $\mathbf{R}$  is the orientation matrix expressing the accelerometer's coordinate frame  $\Psi_s$  in global coordinate frame  $\Psi_g$ .  $\tilde{\omega}_{s,g}^s$  is a skew-symmetric matrix representing the angular velocity, being measured by a 3D rate gyroscope, of sensor frame  $\Psi_s$  with respect to  $\Psi_g$  in frame  $\Psi_s$ .

$$\tilde{\omega}_{s,g}^s = \begin{pmatrix} 0 & -\omega_z & \omega_y \\ \omega_z & 0 & -\omega_x \\ -\omega_y & \omega_x & 0 \end{pmatrix} \quad (3.5)$$

In order to use the identification algorithms either the acceleration, available in global coordinates, needs to be expressed in the force sensor frame or force is to be expressed in global coordinates.

The experimental setup is depicted in 3.7a and 3.7b. It consisted of a handle, instrumented with the IMU from Xsens, rigidly and closely connected to a 6 DOF force/moment sensor unit (ATI-Mini45-SI-580-20, Schunk GmbH & Co. KG). The force/moment sensor was mounted between handle and load, measuring the force and moment that both bodies exerted on each other at the interface.

Experiments were performed with a mass and spring load. The weight of the mass load was 9.37 kg. It was repeatedly lifted from ground onto a 0.75 m high table. Three kinds of movements were applied. First was a minimal rotation during the transition (condition a). Second was a pendulum like movement without applying moment to the handle (condition b). And final movement condition was a tilted transition (condition c).

The spring load was an extension spring (Tevema T39210) with a spring constant of 87.9 N/m and a zero force length of 1.0 m. The lower end of the spring was attached to a vertical iron construction beam 0.15 m from the ground, the other side to the instrumented handle. The handle could be secured to either of two hooks fastened to the construction beam at different heights with respect to the ground: 1.85 and 2.34 m. The handle was repeatedly moved from the lower hook, extended, and secured to the upper hook (condition d). All condition where repeated 19 times.

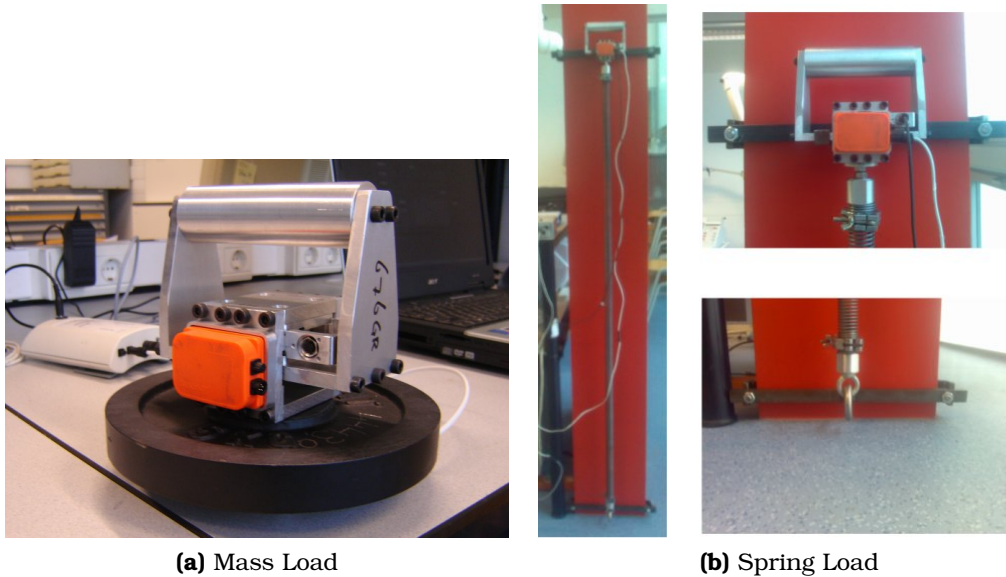


**Figure 3.7.:** Experimental setup with mass and spring load. Between handle and load, the 3D force/moment sensor is mounted. The 3D inertial sensor is visible in orange



## 4. Experimental evaluation results

This chapter presents the results of hapticmaster and physical load experiments. The hapticmaster experiments have been conducted by eight subjects, performing three different kinds of arm tasks. Physical load experiments were conducted by one subject and performed with a mass and a spring load.

After an evaluation of the hapticmaster's load simulation performance, experimental results of three different conditions will be discussed. During the conduction of experiments, the subject's task performance has been evaluated. Thereafter system dynamics of simulated loads were estimated using different algorithms as being discussed in previous chapters. Evaluation of body responses has been performed in the second ('Throw Object') and third ('Punch Bag') hapticmaster condition.

Final part of this chapter gives an analysis of physical load experiments. Task performances have not been evaluated during these experiments.

### 4.1. Evaluation hapticmaster's performance

As discussed before in the method chapter, the hapticmaster is an admittance controlled haptic robot. According to its specifications and reviews (35) the hapticmaster should be able to accurately simulate a wide variety of second order loads. In order to verify the load simulation abilities, different initial tests were performed.

The admittance control paradigm sounds 'force in position out'. This implies that the analysis of rendered output movement gives an indication of the hapticmaster controller's load simulation performance. The end effector has been instrumented with an accelerometer to measure accelerations and estimate velocities and positions. Since the hapticmaster is not instrumented with an accelerometer, velocity signals should be differentiated to estimate accelerations.

In a first performance test, the inertia to be simulated was set to 10 kg. The subject applied forces to the end effector which resulted in planar circle shaped movements. Output accelerations measured by the accelerometer and estimated using the hapticmaster's velocity output are depicted in 4.1.

As visible, measured and estimated accelerations correspond reasonably in magnitude. RMS differences is  $0.42 \text{ m/s}^2$  in x direction and  $0.47 \text{ m/s}^2$  in y direction. A large contribution to these difference is a lag of the accelerometer signal of approximately 40 ms. Shifting the mentioned signal with calculated delay result in an RMS difference of respectively  $0.20 \text{ m/s}^2$  in x direction and  $0.34 \text{ m/s}^2$  in y direction.

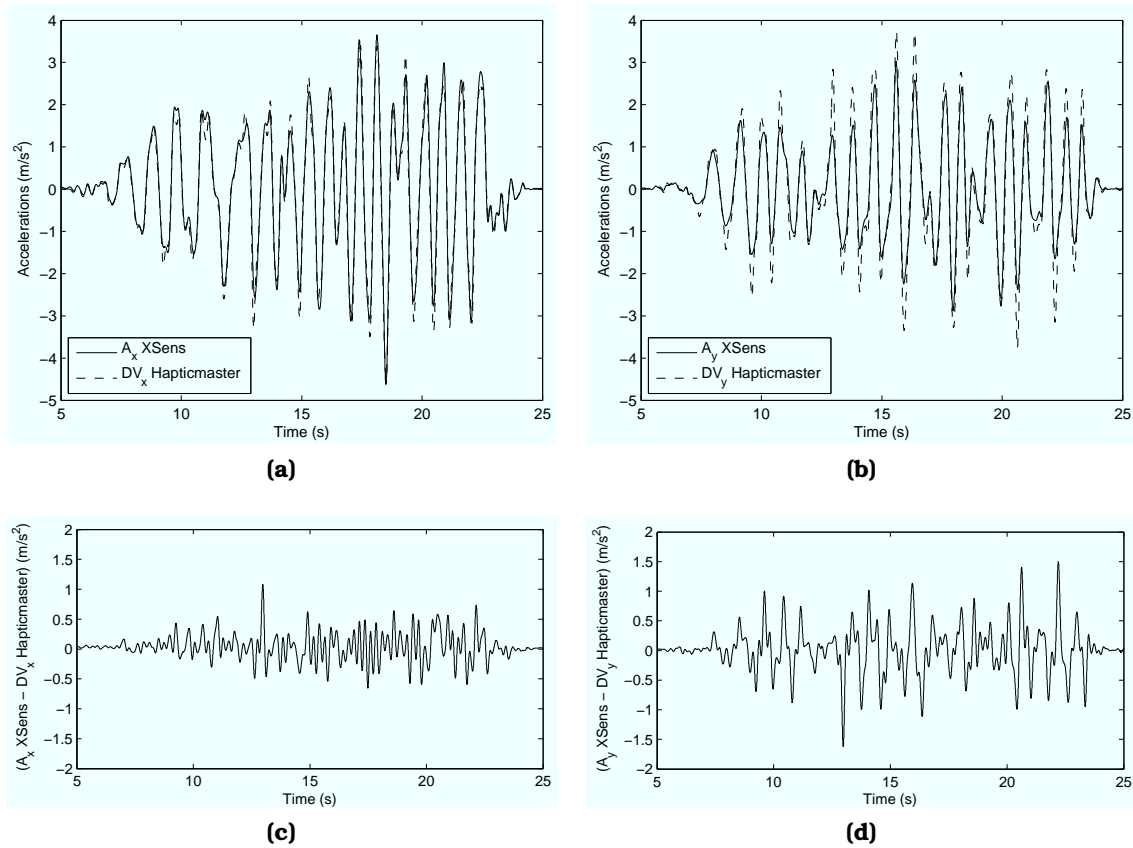


**Figure 4.1.:** Hapticmaster performance results. Forces were actively applied to the simulated load (10 kg mass) resulting in circle shaped movements. Each plot contains accelerations obtained from respectively the attached accelerometer measurements, and the differentiated hapticmaster's velocity. Upper plots shows acceleration in x direction 4.1a and y direction 4.1b. The lower plot show difference between measured and estimated in both directions.

Another clearly visible discrepancy is visible when accelerometer values become maximal in both directions. Estimated acceleration by the hapticmaster velocity show larger peaks than obtained by the accelerometer. This phenomena is predominantly visible in y-direction.

To evaluate relatively short movement tasks, about 1 second, trials of the task condition 'Displace Object' have been evaluated. Again estimated and measured accelerations are compared. Two trials were chosen to clarify notable hapticmaster characteristics. System identification results of this task are given in the next subsection.

In figure 4.2 two trials are depicted. Both are planar movements over approximately 23 cm. Simulated inertias were 10 kg (figure 4.2a) and 5 kg (figure 4.2c). Since subjects were instructed to minimize the transition time, the movement with 5 kg mass load obviously resulted in higher accelerations compared to the 10 kg mass load.

Visualized are the unfiltered accelerometer data, filtered accelerometer data and

estimated accelerations, obtained from hapticmaster velocity measurement. Furthermore the difference of both filtered accelerations is given. The accelerometer data has been filtered using a 5th order low-pass butterworth filter with a cut-off frequency of 5 Hz.

The relatively small acceleration trial (figure 4.2a) displays a remarkable large sinusoidal component, measured in y direction, of approximately 11 Hz. The power spectral density (PSD) of unfiltered accelerometer signal, depicted in figure 4.2b confirms this artificial component. The PSD of accelerations in x direction does not show this approximately peak of 10 dB above the noise level, which indicates that the problem only exist in y direction.

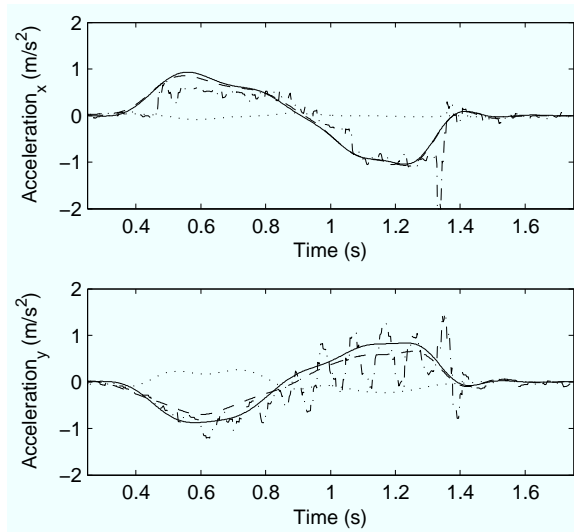
An equivalent trial of the 'Displace Object' condition, depicted in figure 4.2c, with a 5 kg mass load show larger acceleration magnitudes. This is furthermore visible in figure 4.2d where acceleration signal power below 3 Hz is larger compared to the 10 kg trial. Remarkable in the acceleration plot and PSD of latter trial is the absence of undesired 11 Hz interference in y direction, which suggests that small acceleration movements, cause an increase in spectral power of this 11 Hz component. This could be designated to the admittance controller of the hapticmaster, that is operating close to instability.

Next, the accelerometer signal of both trials show a large peak at respectively  $t=1.4$  s and  $t=1.6$ . This can be explained by a sudden increase in damping, as being commanded to the controller, when the measured velocity magnitude drops 0.05 m/s at the end of the movement.

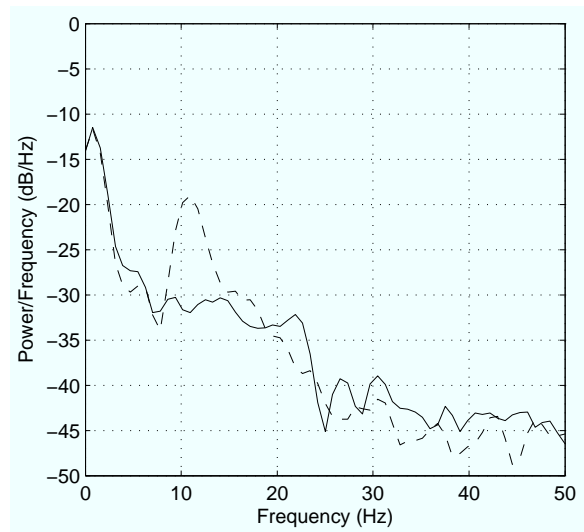
Largest acceleration differences are visible in y direction. Probably caused by the 11 Hz interference, since it is only present in this direction.

In addition measured forces are compared to reconstructed forces according equation 2.5. Simulated inertia and damping was to respectively 10 kg and 10 Ns/m. Reconstruction of total force was performed using differentiated velocity signals of the hapticmaster (figure 4.3a). The difference in measured force and reconstructed was smaller compared to the situation where total force was reconstructed using measured accelerations (figure 4.3b). Latter are shifted by the calculated delay, indicated in first subsection of this chapter. The largest discrepancies are visible in the Y direction.

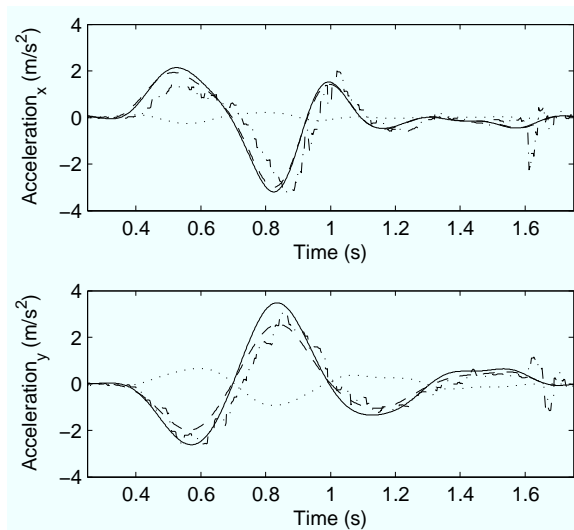
Possible explanation would be that the hapticmaster position and velocity output signals are calculated using the internal admittance model and are therefore inherently dependent of the measured forces. An error in measured forces results in an error of the calculated movement, but will effectively have the same magnitude.



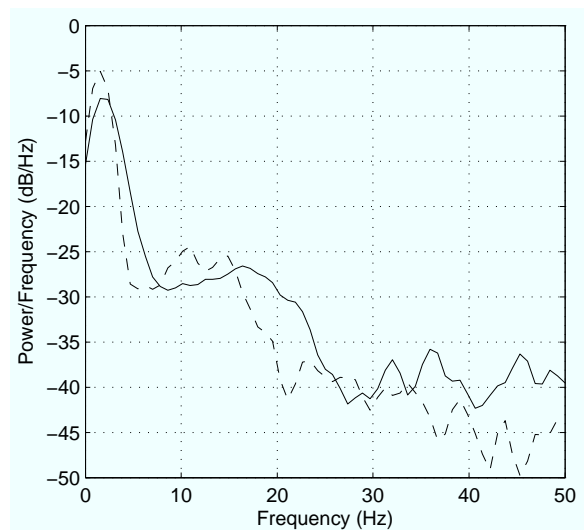
(a) Low acceleration trial with 10 kg mass load (upper x, lower y direction)



(b) PSD of raw accelerometer signal of 4.2a. X direction is solid, Y direction is dashed.

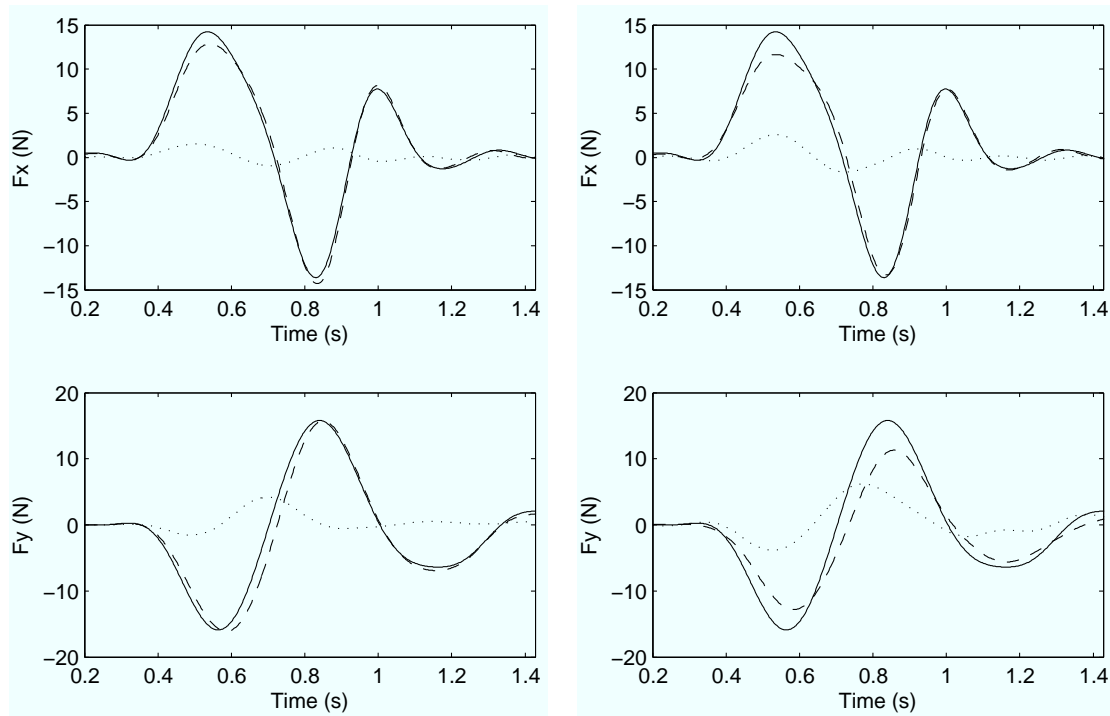


(c) High acceleration trial with 5 kg mass load (upper x, lower y direction)



(d) PSD of raw accelerometer signal of 4.2c. X direction is solid, Y direction is dashed.

**Figure 4.2.:** Acceleration profiles of two ‘Object Displacement’ task trials. On the left side x and y direction of both trials with unfiltered accelerometer (dashed-dotted), filtered accelerometer (dashed) and filtered differentiated hapticmaster (solid and difference between filtered accelerometer and hapticmaster (dotted)). The plots on the right show the power spectral density (PSD) of corresponding acceleration signals.



(a) Differentiated velocity signals of the hapticmaster are used to estimate the accelerations being used to compute the force component caused by accelerated inertia.

(b) Accelerations measured by the accelerometer are used to compute the force component caused by accelerated inertia.

**Figure 4.3.:** Sensed forces (solid), reconstructed forces, according 2.5 (dashed) and absolute difference (dotted).

## 4.2. Displace Object task, simulated mass

First task instructed to the participants is the 'Dispace Object' task. Instructions have been described in section 3.1.1. A screenshot of the corresponding user interface is given in figure 3.5. In figure 4.4 movement trials are visualized of an arbitrary subject. The average movement duration was 1.8 second. An example of interface force and movement measurements during one trial is illustrated in figure 4.5.

In figure 4.3a and 4.3b are the measured forces depicted in combination with the estimated forces, which have been computed by multiplication of sensed kinematics with parameters of simulated second order dynamics, see equation 2.5.

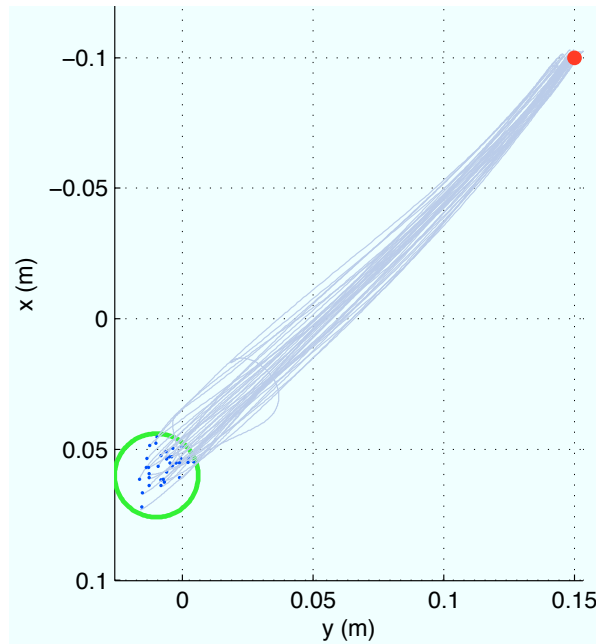


**Figure 4.4.:** Trial trajectories of the 'Displace Object' task. The starting position is indicated by the upper right red dot . The prescribed end position is the inner area of the lower left circle circumference which has been marked in green. Actual end positions are illustrated by a blue dot. Only trials which met the prescribed conditions are drawn. Task instructions and conditions can be found in table 3.4

### 4.2.1. Evaluation of task performance

The task performance has been evaluated while the specified task was executed by the participant. The interface as shown to the subjects (figure 3.5a), is equipped with two text lines showing the highscore and actual score. Movement trials have been judged using criteria of which the subject was informed before start of the experiments.

The 'Object Displacement' task instructions sounds: 'Move the load from a to b in a minimum amount of time'. Next, the computed score is a function of the inverse of displacement duration.

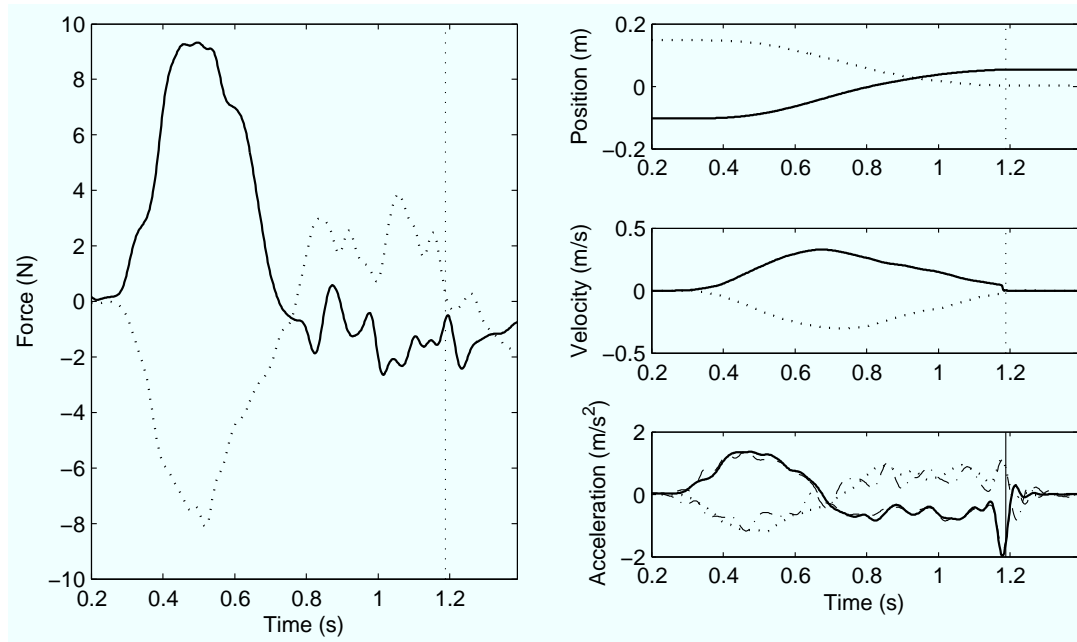


**Figure 4.5.:** Sensed forces, positions and accelerations of 'Displace Object' task during one trial in x (solid) and y (dotted) direction. Load dynamics consists of a 10 kg mass and 10 Ns/m viscous damper. Furthermore the estimated velocities and accelerations are given. The vertical dashed line indicates the end of the movement.

In figure 4.6 a scoring chart is depicted of an arbitrary subject. The results indicate that evaluation of task performance is feasible using force and movement measured at the interface between body and environment. Analysis of performance trends is not part of this study.

#### 4.2.2. Identification of system dynamics

Dynamics of simulated loads are estimated using the 'ARX', 'Prediction Error Method' and 'Subspace' system identification algorithms which have been discussed in the background chapter. All algorithms used the measured force and position signals as input. The ARX model structure is linear in the parameters and estimation is therefore possible by a fast least squares algorithm. The subspace method uses the state space description and a non iterative algorithm to calculate the parameter values. In contrast to 'ARX' and 'Subspace' methods, the 'Prediction Error' method does an iterative search in the parameter space.

For this method, a canonical model structure has been defined in order to limit the number of parameter to be estimated. The state space description can be found in equation 2.26. The matrixes of A,B,C,D and K have to be estimated. Because prior knowledge of the system is known (see equation 2.9 and 2.9) we fixed the following parameters to their known values:

$$A = \begin{bmatrix} 0 & 1 \\ a_{2,1} & a_{2,2} \end{bmatrix}, B = \begin{bmatrix} 0 \\ b_{2,1} \end{bmatrix}, C = [1 \ 0], D = 0, K = \begin{bmatrix} k_{1,1} \\ k_{2,1} \end{bmatrix} \quad (4.1)$$

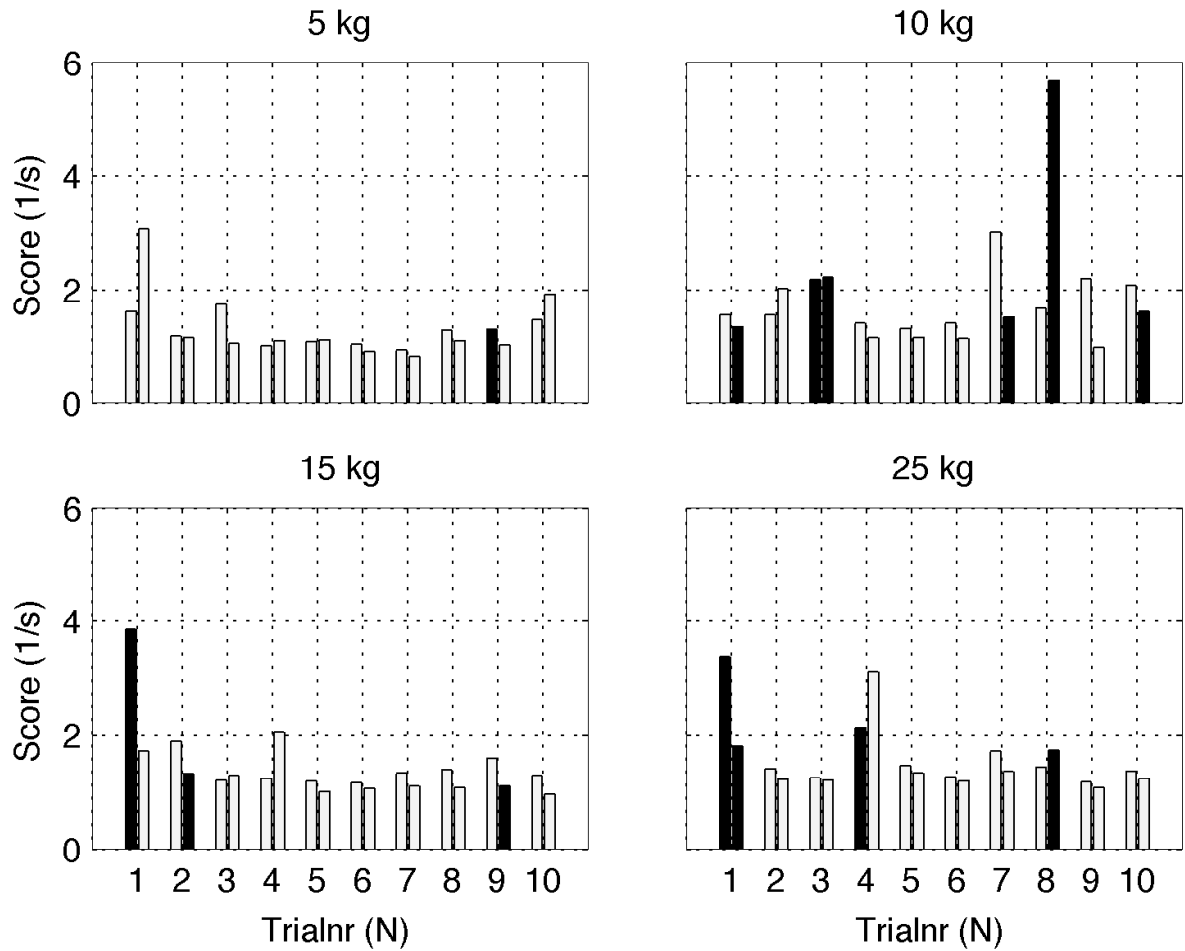


**Figure 4.6.:** Task performance of an arbitrary subject. Scoring values are determined by durations of the movement. Lower values indicate a better score. Bars are grouped by two trials illustrating the repetition of corresponding trial. Black bars indicate trials which did not satisfy any of the boundary conditions.

Now the parameter space is spanned by the unknown parameters. In addition prior knowledge of the (second order) system resulted in the initial values of respectively  $a_{2,1} = a_{2,2} = -1$  and  $b_{2,1} = 1$ .

Next the PEM algorithm iteratively tunes the parameters in order to minimize the cost function described in equation 2.22 and 2.23 using a LevenbergMarquardt search algorithm.

An optimal model order is determined by calculating the singular value decompositions of different orders, see figure 4.7. The largest discrepancy is visible between the singular values of second and third order, indicating second order is optimal.

Next the estimated models were used to calculate the estimated position (as the position being the output of estimated model) in both X and Y direction. Both direction have been separated because of the deteriorated rendering capabilities in Y direction.

Positions for a random trial have been visualized in figure 4.8. Visible are both measured and estimated output positions. The ARX and subspace methods show good correspondence to the measured positions. Only in Y direction the subspace outperforms the ARX method. The prediction error method estimate less accurate the output profile. This can be explained by the fact that the 'Prediction Error' method uses a canonical model structure.

The predication error methods require an analysis of the model residuals, see section 2.5.5. The upper plot of figure 4.9 depicts the autocorrelation of model residuals for an arbitrary trial in X direction. Visible is that the iterative PEM method' residuals are slightly better uncorrelated compared to ARX. Correlations which exceed the confidence interval implies that not all dynamics are fully captured by the estimated model.

The lower plot in figure 4.9 depict the cross correlation between output residuals and past model inputs. The least squares method (ARX) constructs the parameter vector  $\theta$  so that the residuals are uncorrelated with the regressors (model inputs). Which means that the cross-correlations are automatically zero. In case of the iterative PEM method, correlations fall within the confidence intervals. This implies that delays are correctly estimated and no feedback is present.

Estimation by means of a recursive method were unsuccessful during these short interaction. In the bottom plots of figure 4.10a and 4.10b, recursively estimated discrete parameters combined with actual values were plotted for two trials. Upper and middle plot of both figures show the input and output which have been fed to the recursive algorithm to identify the system dynamics. Algorithm used was the Recursive ARX method as described in section 2.4.4.1 in combination with a forgetting factor approach, with a typical lambda of 0.99.

In figure 4.10a the general trend of all recursively identified trials is illustrated: Parameter values did not converge to their actual values (illustrated by solid lines), but at least they are seeking to the right direction. In figure 4.10b an occasional

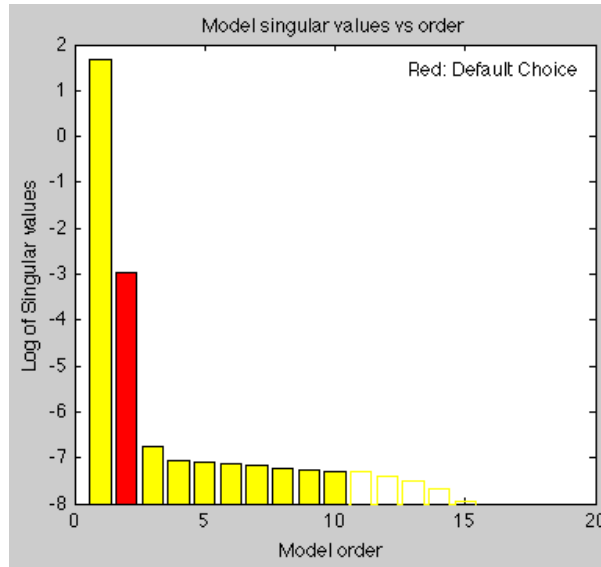


**Figure 4.7.:** Singular value decompositions versus the model order. Largest discrepancy is visible between third and second column, which indicate that a second order model structure will probably sufficient to capture the all most important dynamics.

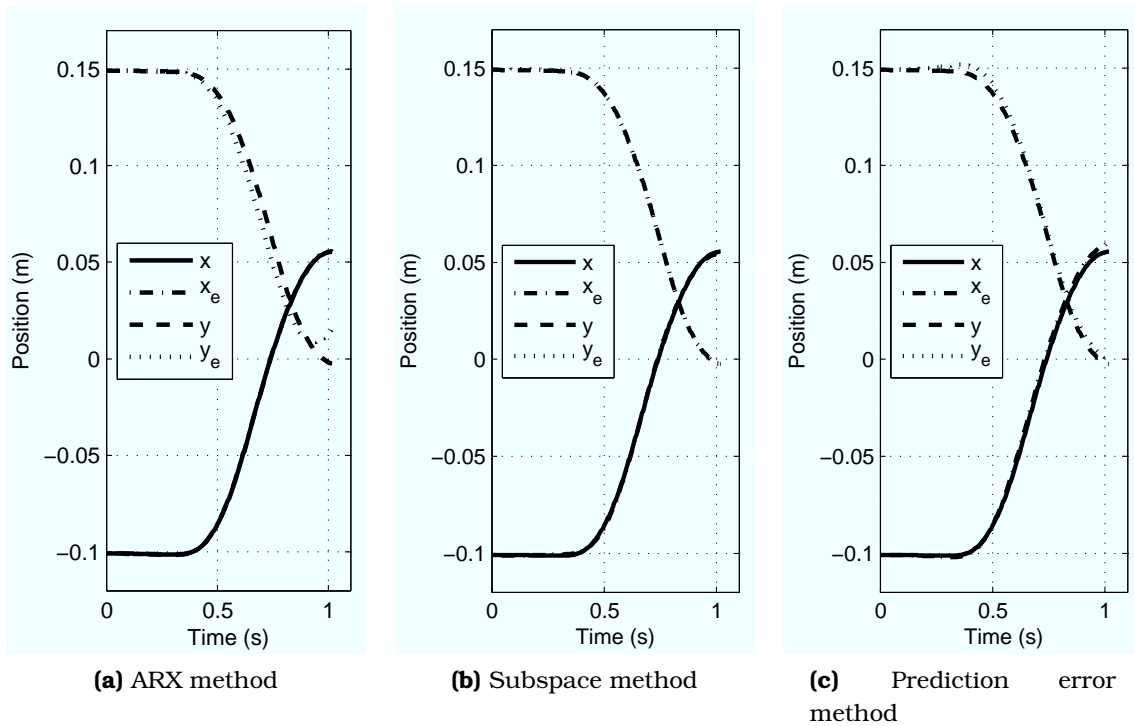


**Figure 4.8.:** Output position in both x and y direction of the 'Displace Object' task. Estimated positions  $x_e$  and  $y_e$  are calculated using the identified models by different identification algorithms.

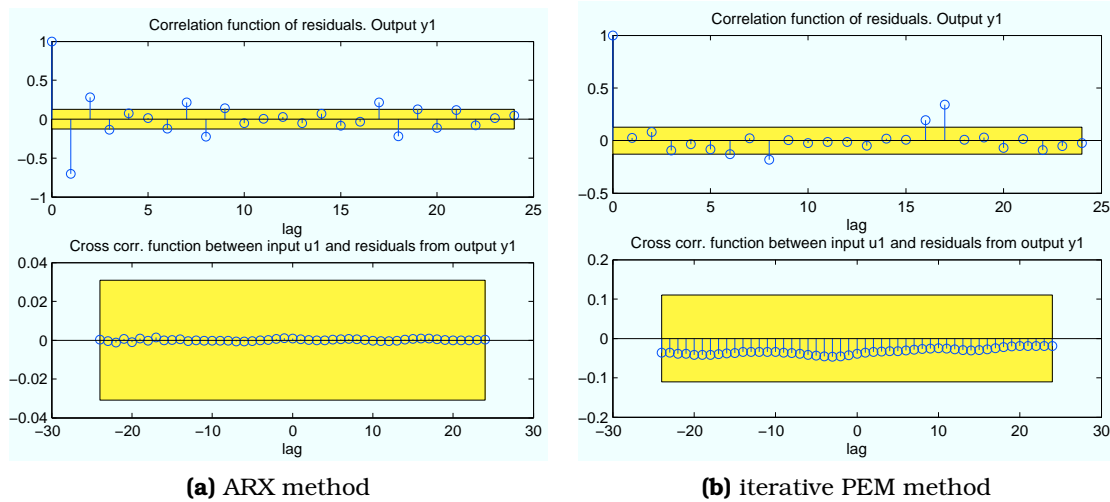


**Figure 4.9.:** Residual analysis of arbitrary trial ‘Displace Object’ trial in X direction. Upper plots are auto correlations of model residuals and lower plots are cross correlations between model inputs and residuals.

successful identification result is shown: the parameter vector is converging to the real system parameters.

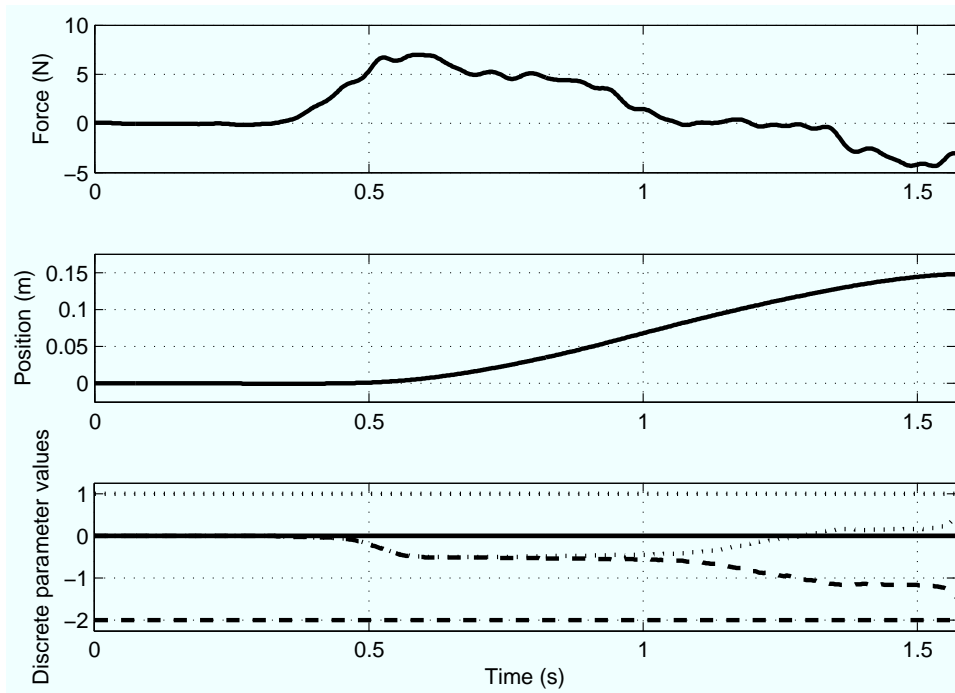
A statistical analysis has been performed for all non-recursive identification algorithms. This will give information about the quality of estimated parameter values and characterizes the load simulation capabilities of the hapticmaster.

Eight subjects performed 80 trials each, divided over 4 groups with four different (5, 10, 15 and 25 kg) simulated end-effector inertias. Hence each simulated mass contains 160 unique trials. Table 4.1 summarizes the estimated inertia values and error values for every inertia and identification method. Mean error values and standard deviations are significantly lower for X direction with respect to Y direction for all identification methods. For the X direction: The Prediction error method outperforms all methods. It shows the smallest error in estimating the mass parameter. The subspace method show better mean values but employs larger standard deviations compared to the ARX method.

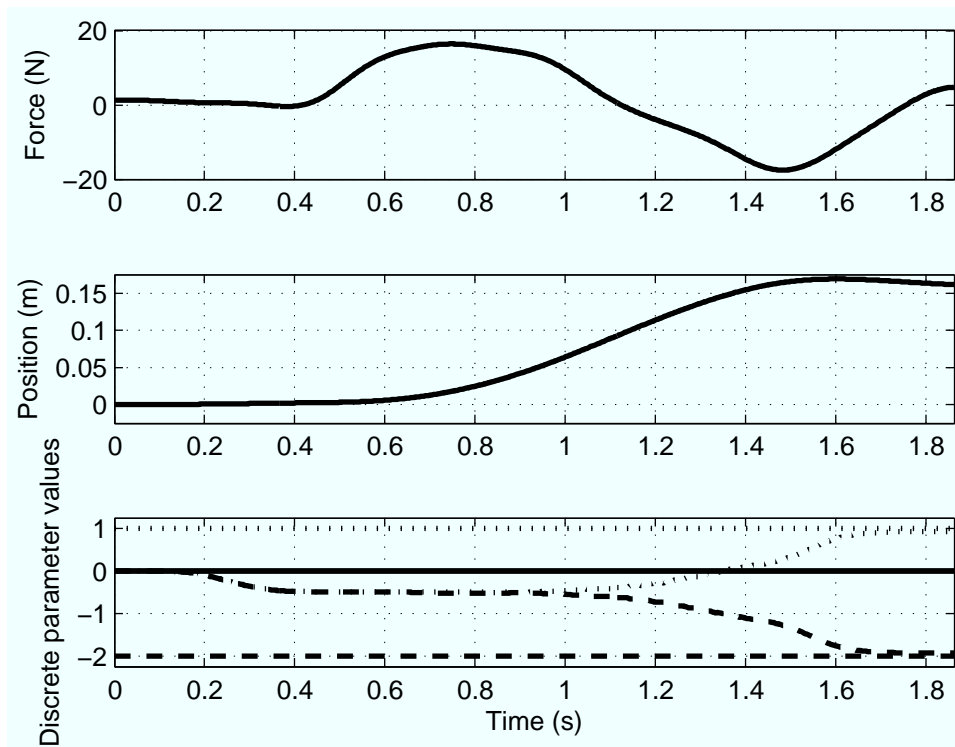
Figure 4.11 show box whisker plots of estimated mass values for different identification methods and movement directions.

Mass (kg)	Duration (s)	ARX				Prediction Error				Subspace			
		X		Y		X		Y		X		Y	
		Est. M(kg)	Err.(%)	Est. M(kg)	Err.(%)	Est. M(kg)	Err.(%)	Est. M(kg)	Err.(%)	Est. M(kg)	Err.(%)	Est. M(kg)	Err.(%)
5	1.6 ± 0.9	5.3±0.8	6.4±16.2	4.6±9.4	-7.9±18.8	5.2±0.3	3.8±5.8	5.4±0.9	7.2±17.9	5.3±1.9	4.9±38.4	5.4±2.1	8.3±41.6
10	1.8 ± 0.8	10.9±1.2	8.6±12.0	10.0±4.8	-0.1±4.8	10.2±1.0	2.1±9.7	10.6±2.5	5.8±24.8	10.5±2.4	4.8±24.0	10.2±3.7	2.3±36.8
15	1.7 ± 0.7	16.2±1.4	7.4±9.5	12.9±21.8	-16.3±14.5	15.5±1.1	3.0±7.2	15.9±4.4	5.9±29.6	15.1±3.0	0.6±20.2	15.3±7.4	2.2±49.3
25	1.9 ± 0.8	25.5±2.7	1.3±10.9	108.8±1.5e3	77.0±4.2e3	25.0±2.5	0.1±10.0	27.5±5.3	9.1±21.3	24.3±4.8	-2.7±19.2	23.7±9.0	-5.4±35.9

**Table 4.1.:** Estimated mass (Est. M) values for different simulated masses using subspace and prediction error and ARX method. Four different simulated inertias are evaluated in both X and Y direction of the ‘Displace Object’ task.



(a) Unsuccessful recursive identified dynamics



(b) Successful recursive identified dynamics

**Figure 4.10.:** Recursive identification of two trials (a and b). Both trials show three plots, upper and middle plot shows the measured force and position in X direction respectively. Both are used for the recursive algorithm where former is used as model input and latter as model output. Bottom plot show the estimated discrete parameter values as function of time. Actual real values are depicted with horizontal lines.

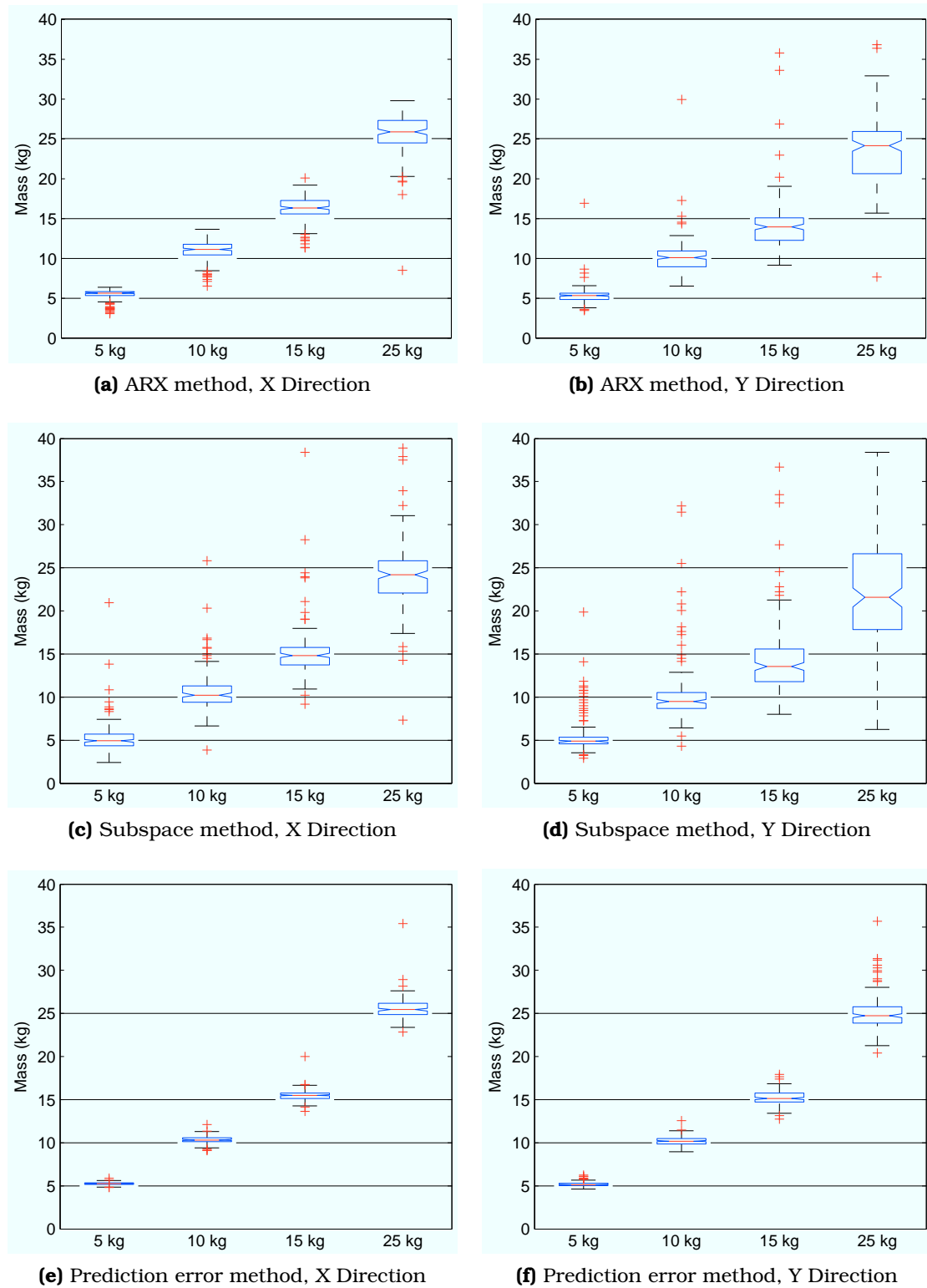


**Figure 4.11.:** Box-whisker plots of estimated mass values in 'Displace Object' task. Central mark is the median, the edges of the box are the 25th and 75th percentile, whiskers extend to the most extreme data points whereas outliers are plotted individually. Actual values are highlighted using horizontal lines. In descending row order the are the results of the following identification algorithms depicted, 'ARX', 'Subspace' and 'Prediction Error Method'

### 4.3. Throw Object task, abrupt reduction of simulated mass

The second task performed by the participants is the 'Throw Object' task. This task can be characterized by a sudden decrease in load inertia while the subject applies force to the mass load. The force appliance resulted in a planar hand-load movement of approximately 20 cm. Important consequence is that load dynamics cannot be considered to be linear over the total transition. Task instructions have been described in section 3.1.2. A screenshot of the corresponding user interface as being displayed to the subjects is depicted in figure 3.5b. In figure 4.12 movement trials are visualized of an arbitrary subject. An example of interface force and movement measurements during one trial is illustrated in figure 4.13.

Figure 4.15 shows the measured and estimated forces, which have been computed by multiplication of sensed kinematics and parameter values of simulated second order dynamics, see equation 2.5. The vertical dashed line indicates the inertia transition. The simulated inertia was decreased from 25 kilograms to 2 kg, which is the least possible inertia which can be simulated by the hapticmaster. Similar to the other hapticmaster tasks, 4 different initial masses have been evaluated (5, 10, 15 and 25 kilograms).

Figure 4.14 depicts the interface forces, velocities and accelerations of two (5 and 25 kg) simulated inertias. Throughout all trial observations, a few things are remarkable. First we notice the conservation of momentum. When the inertia suddenly drops, we immediately see an increased velocity, which is obviously depended of the difference in inertia before and after the decline.

Responses after the inertia transition are predominantly available when the difference in inertia was large. In the observed trials we notice an oscillation like phenomena in y direction of the accelerations. In figure 4.14b this is visible between the vertical discontinuity line at  $t=1$  s. Furthermore we notice that the acceleration in x direction remains constant for a while and disappears after approximately 0.1 s. Both observations are mainly visible in trials with the 25 kg mass loads.

Evaluation of the subject task performance has been carried out while participants performed the task. The score was determined by the impulse value on transition from higher to lower inertia. Impulse is the product of simulated inertia en measured velocity.

#### 4.3.1. Identification of system dynamics

Because the participant is subjected to load discontinuities during the task execution, mentioned identification methods result in erroneous estimations of parameter values. Therefore movement trials are a split up in parts where the participant was not subjected to this non linearity, thus simulated loads can be regarded to be stationary. Identification of linear parts is now possible but require the time of occurrence of this discontinuity. Second strategy is the usage of a recursive identification algorithm which can track parameter fluctuations. Unfortunately this algorithm was

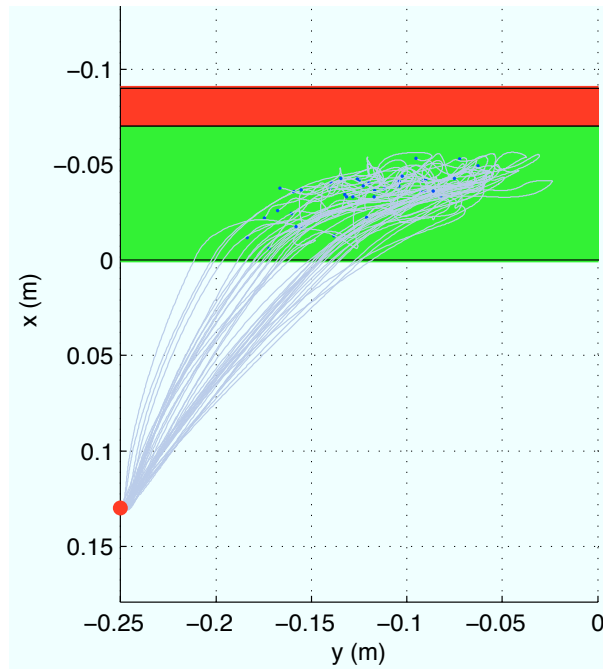


**Figure 4.12.:** Trial trajectories of the ‘Throw Object’ task. The starting position is indicated by the upper left red dot. Subjects moved their right arm away from the sagittal plane of the body (abduction). Only movement in transverse plane were allowed. When the hand surpasses  $x=0$ , which is similar to the green line in figure 3.5b, simulated end effector inertias have been lowered significantly. Movement end points, indicated in blue, ended up somewhere in the green area. Subjects were instructed not to enter the red area, see also 3.5b. When this requirement is violated, the concerned trial will be rejected, and is therefore not drawn in this plot. Task instructions and conditions can be found in table 3.4

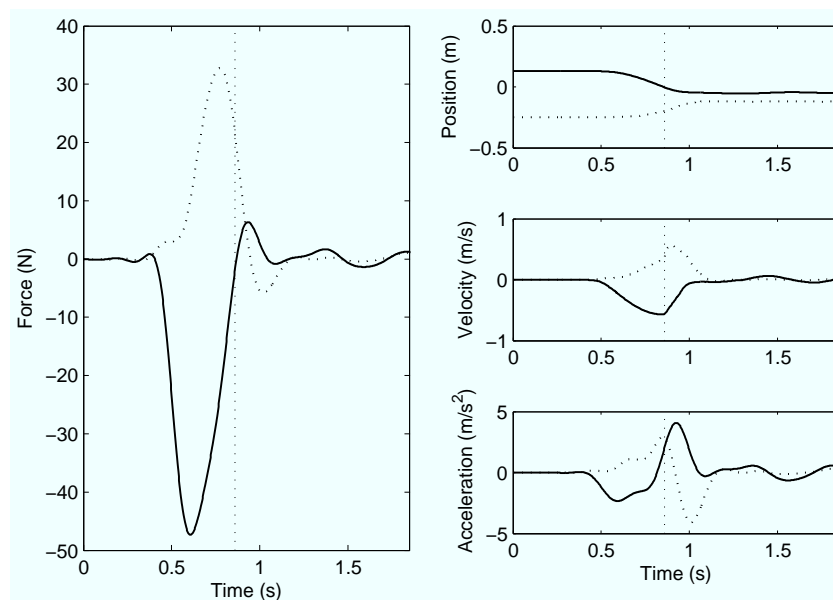


**Figure 4.13.:** Sensed forces, positions and accelerations of ‘Throw Object’ task during one trial in x (solid) and y (dotted) direction. Load dynamics includes a 25 kg mass and 10 Ns/m viscous damper. Furthermore the estimated velocities and accelerations are given. The vertical dashed line marks the decrease in simulated inertia.

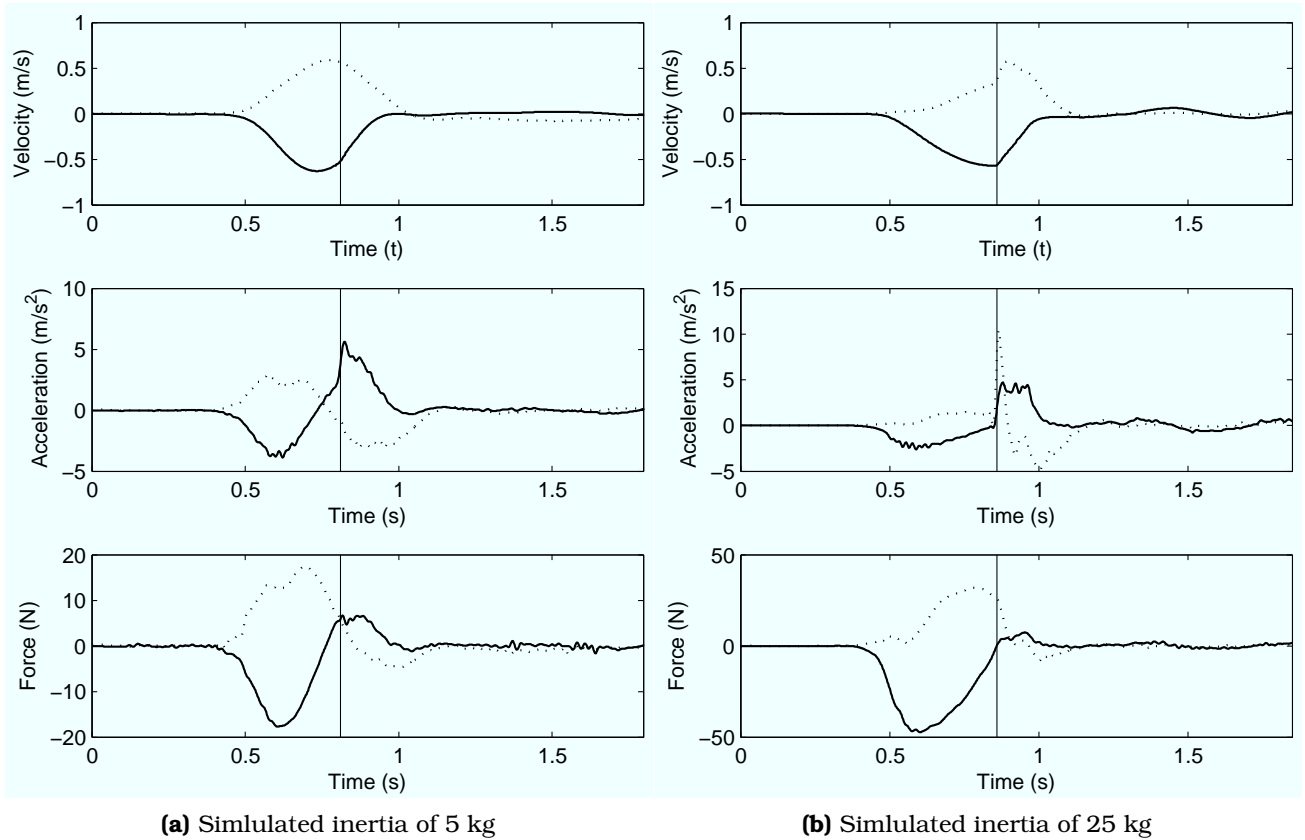


**Figure 4.14.:** Velocity, Acceleration and Force plots of two 'Throw Object' movements in both X (solid) and Y (dashed) direction.

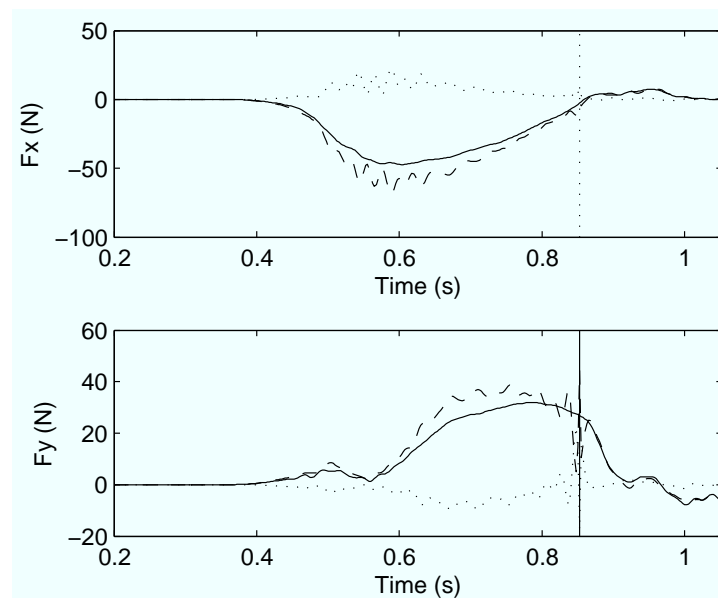


**Figure 4.15.:** Sensed forces (solid), estimated forces (dashed) and absolute difference (dotted). Differentiated velocity signals of the hapticmaster are used to estimate the accelerations being used to compute the force component caused by accelerated inertia.

not able to estimate parameter in the previous 'Displace Object' condition. This gives a plausible reason that the recursive identification algorithm were not able to estimate dynamics during this condition, because the period in which loads can regarded to be linear was shorter compared to the durations of 'Displace Object' movements.

Figure 4.16 show box-whisker plots of the estimated masses before and after lowering the inertia to 2 kilograms. Because the 'Prediction Error' method gave better results than the 'Subspace' and the 'ARX' method only the former algorithm is used to create the plots.

Remarkable facts are the apparent strong biased estimates in X direction visible in 4.16a. The data in Y direction show a much larger extend compared to X direction, see 4.16b. These large discrepancies are probably caused due to the fact that the movement, before inertia is decreased, was primary in Y direction. Which implies that the information extend of force and movement measurements is larger in Y direction than X. Trial recording length average was 0.8 s for the lowest initial inertia (5 kg) and 1.1 s for the highest initial inertia. Mean reaction time (time between start of recording and movement onset of the subject) was 0.5 s during this task, which implies an effective measurement duration of respectively 0.3 s and 0.6 s. This is significantly less than average duration of the 'Displace Object' task and could thus explain erroneous estimation results.

Part of the movement right after the inertia was lowered resulted in much better load estimations, see 4.16c and 4.16d. This can be explained by larger recording lengths (average of 2 s) where participants had actively applied forces in both X and Y direction.

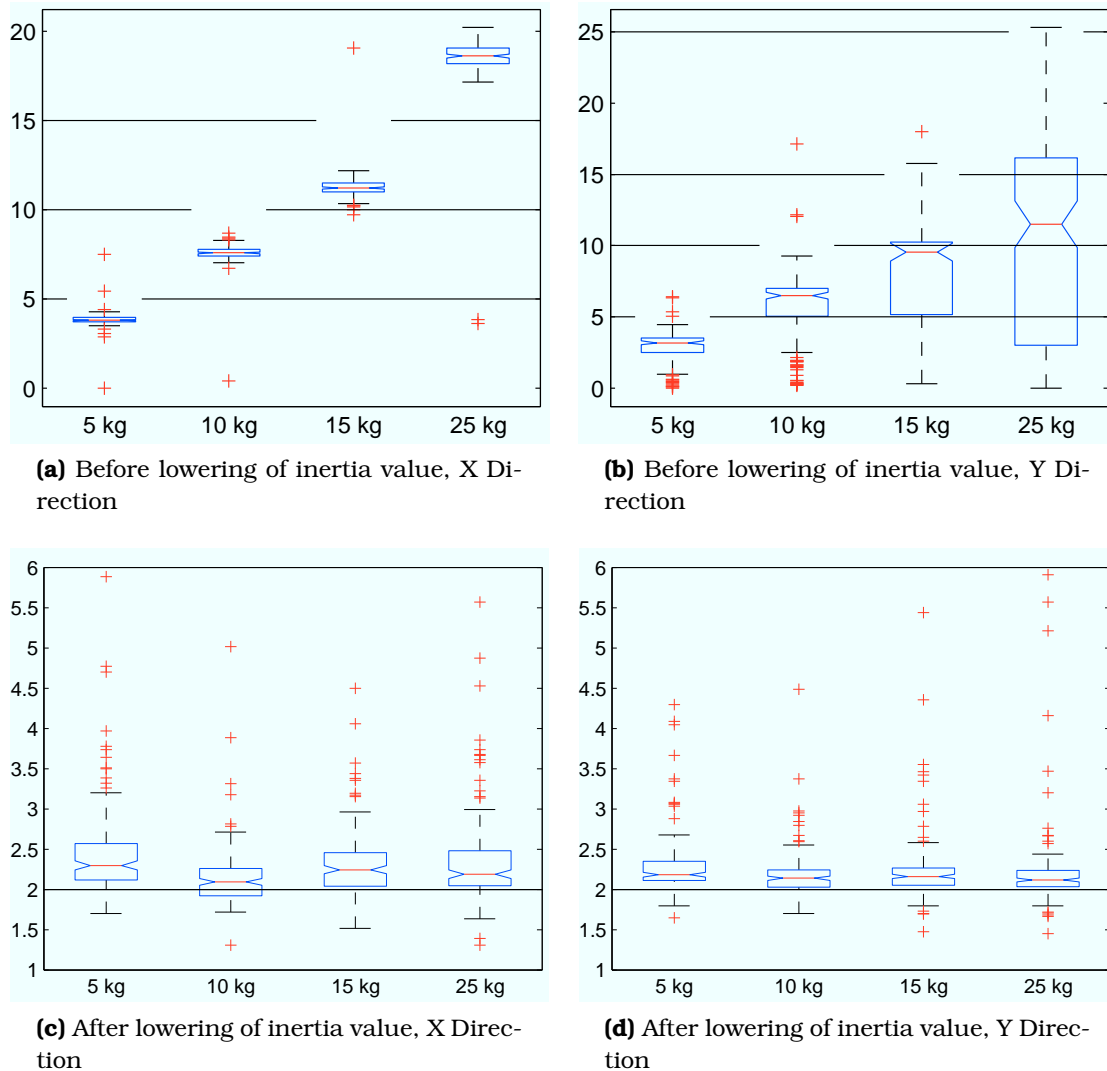


**Figure 4.16.:** Box-whisker plots of estimated mass values in "Throw Object" task. Central mark is the median, the edges of the box are the 25th and 75th percentile, whiskers extend to the most extreme datapoints whereas outliers are plotted individually. The prediction error method has been used as identification algorithm. Actual values are highlighted using horizontal lines. The upper figure depicts results before the inertia has been lowered to 2 kilograms. Results of latter situation can be found below.

#### 4.4. Punch object task, abrupt rise in simulated viscous damping

Final task performed by the participants is the 'Punch Object' task. This task is characterized by a sudden increase in viscous damping of load dynamics while the subject is performing a movement with the corresponding load. One should take in mind that, similar to the previous task, load dynamics contain a discontinuity over the entire trajectory. A screenshot of the corresponding user interface as being displayed to the subjects is depicted in figure 3.5c. Task instructions are given in section 3.1.3. Trajectories of a random subject are depicted in figure 4.17. The trajectory path length was approximately 21 cm. The position where the subject encountered the sudden damping is depicted by the circumference of the green square.

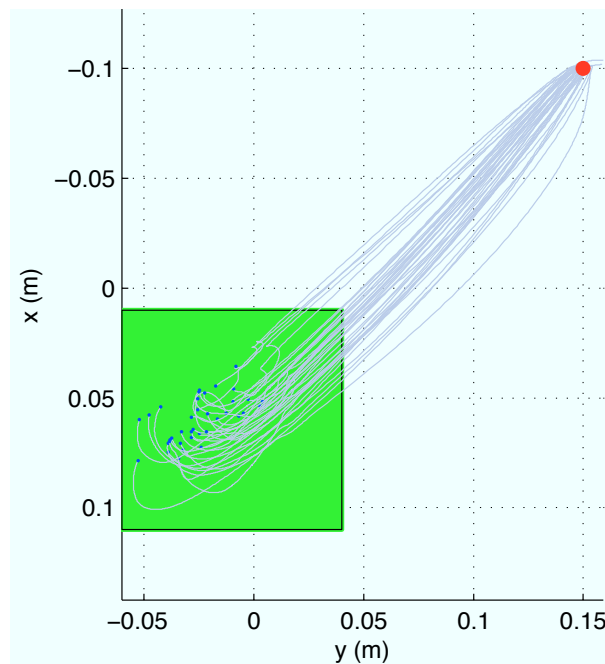


**Figure 4.17.:** Trajectories 'Punch Object' task. The starting position is indicated by the upper right red dot. Subjects moved their right arm to the sagittal plane of the body (adduction). Only movement in transverse plane were allowed. When the hand surpasses the boundary of the green box (see also figure 3.5c), simulated viscous damping rised significantly. Movement end points, indicated in blue, ended up somewhere in the green area.

Figure 4.19 shows the measured and reconstructed forces (see equation 2.5) for a simulated mass of 5 kg. A large error is visible after impact. Figure 4.18 compares the kinematic and kinetic quantities for a simulated mass of 5 and 25 kg. From this plot one can notice the following characteristics, which are visible throughout the experimental observations.

When the target is hit, the inertia of load and hand will be decelerated, resulting in a simultaneous velocity drop. The applied impulse determines the length of this deceleration phase.

In contrast to the previous 'Throw Object' task, responses are visible in measured interface forces. After the moment of impact a short oscillation like phenomena is visible in X direction of the movement. Especially the low simulated inertias (5 kg) display this oscillation. This underdamped system behavior has a natural frequency about 14 Hz and a damping ratio below one. Described phenomena is primary occurring in X direction and only for low simulated inertias (compare figure 4.18a and 4.18b).

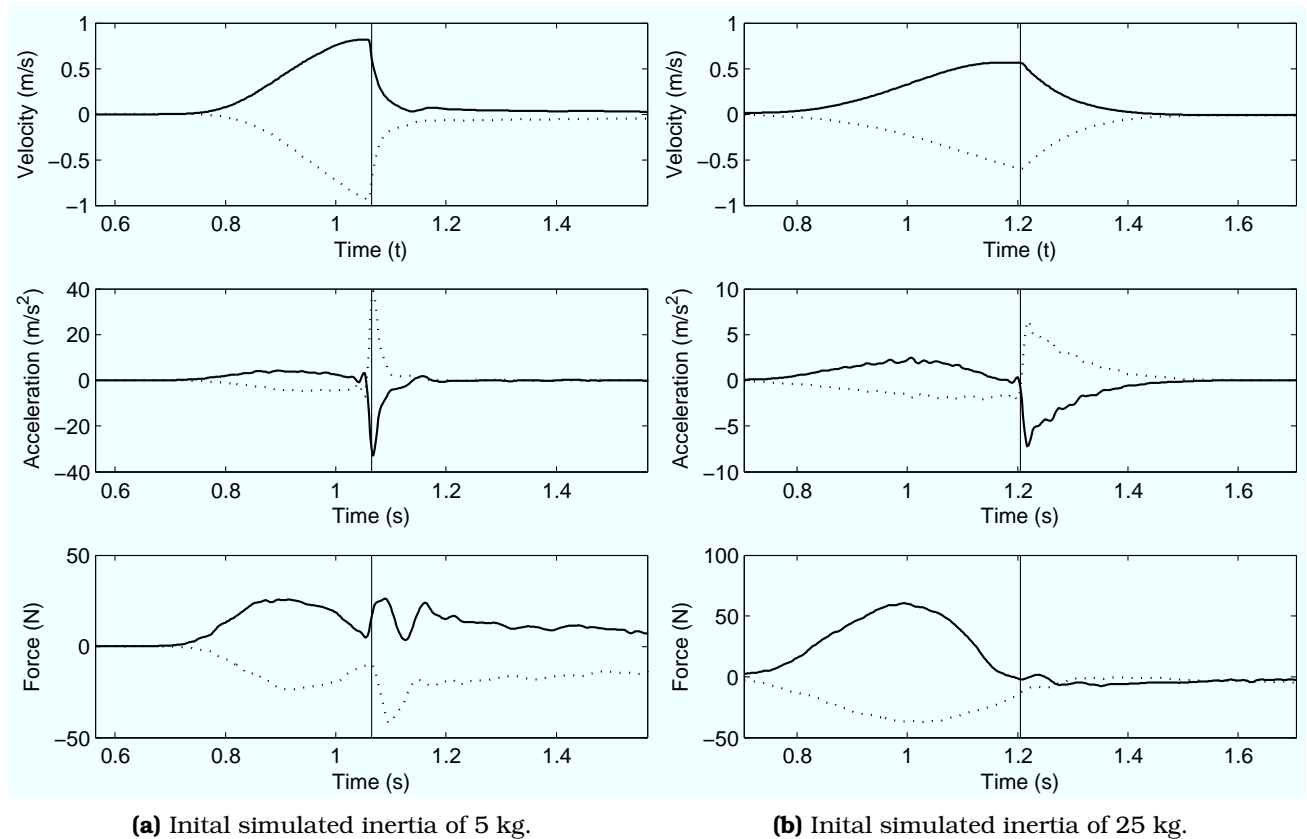


**Figure 4.18.:** Velocity, Acceleration and Force plots of two 'Punch Object' during one movement trial in both X (solid) and Y (dashed) direction. Simulated inertias are 5 kg (upper) and 25 kg (lower). Load dynamics includes a 5 kg mass and 10 Ns/m viscous damper. When the subject 'hits' the viscous object damping has been increased to 300 Ns/m. The vertical dashed line indicates the discontinuity of dynamics.

#### 4.4.1. Identification of system dynamics

Because the discontinuity in load dynamics, the data has been split in a movement before and after the discontinuity onset. Because of the responses visible in the forces, the first 50 ms of data after collision has been rejected. Hence linear identification strategies can now be applied to both records. Figure 4.20 shows box whisker plots of estimated mass values whereas figure 4.21 show the estimated viscous damping parameter, for the situation before and after the discontinuity.

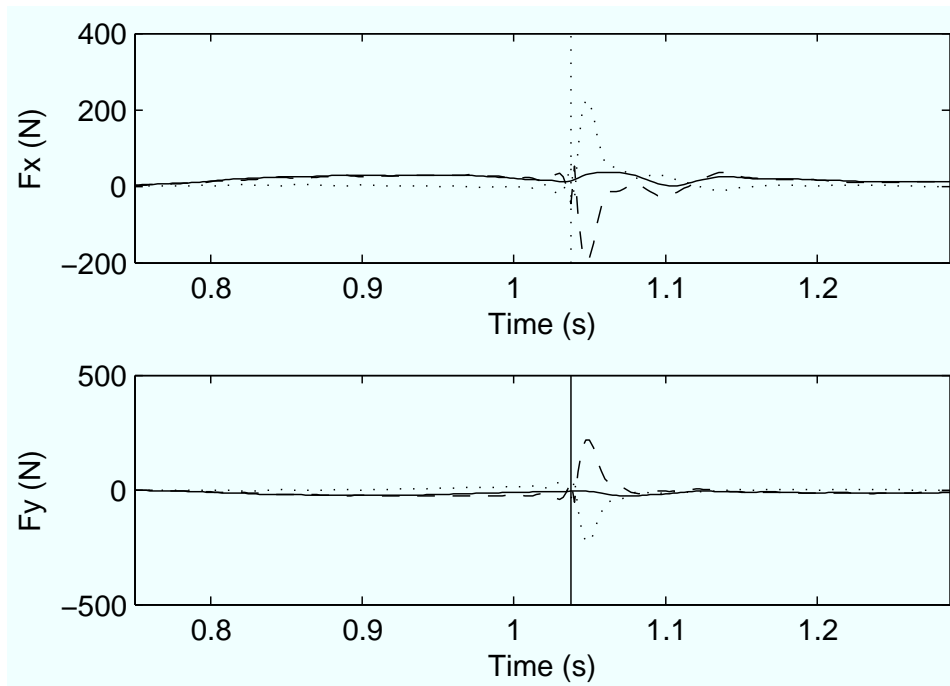


**Figure 4.19.:** Sensed forces (solid), estimated forces (dashed) and absolute difference (dotted) of ‘Punch Object’ task. Differentiated velocity signals of the hapticmaster are used to estimate the accelerations being used to compute the force component caused by accelerated inertia.

Similar to the ‘Throw Object’ task, mass parameter values are biased. Before impact a positive bias is visible whereas after this discontinuity a negative bias is visible. Both are probably caused by the duration of both trajectories.

Estimated damping parameters show a negative trend by an increase in simulated mass (see figure 4.21). Another remarkable fact are the 25th and 75th percentile whiskers when simulated mass was 5 kg after impact. Estimated damping and mass values are much more spread in this situation. As force responses are noticed for this simulated inertia (figure 4.19), interface forces are not completely determined by the load (even when first 50 ms of data after collision was rejected). Hence a discrepancy will be visible in estimated parameters when a second order model structure is considered.

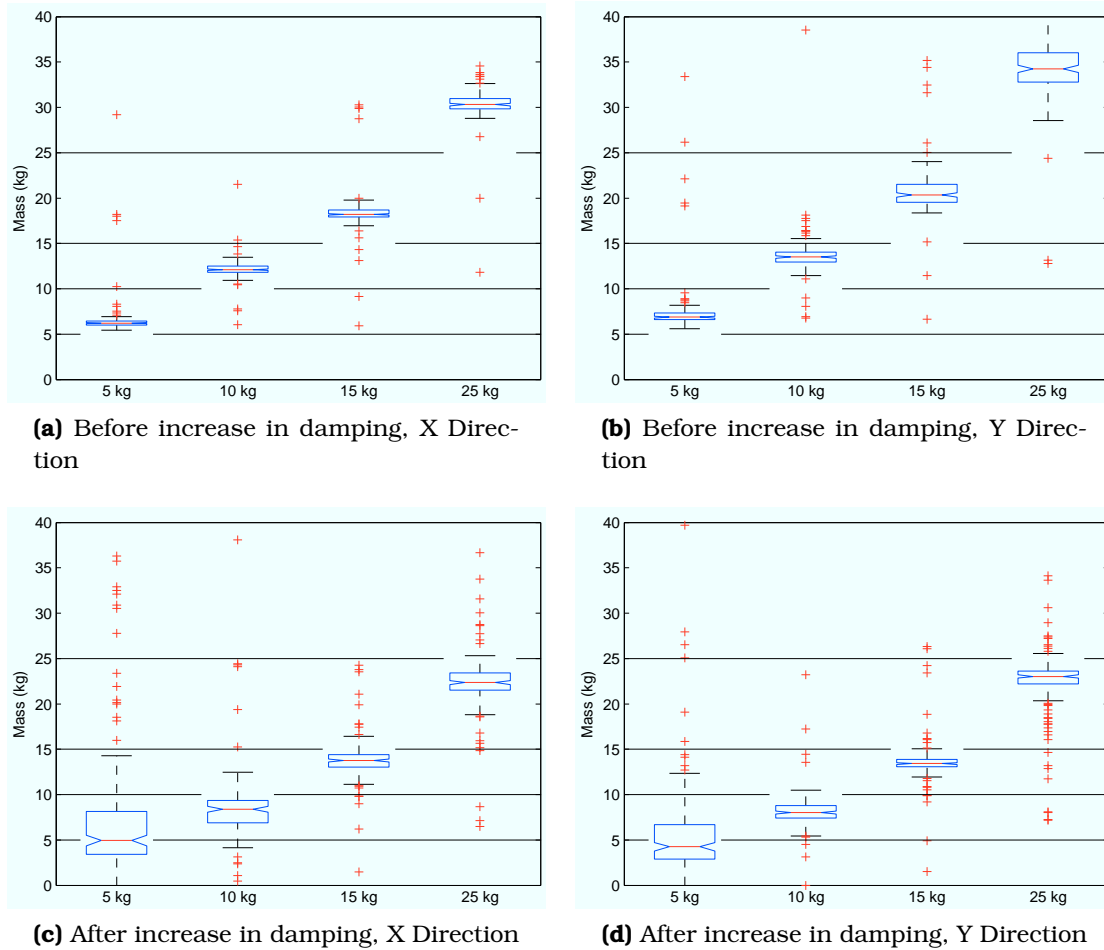


**Figure 4.20.:** Box-whisker plots of estimated mass values in 'Punch Object' task. Central mark is the median, the edges of the box are the 25th and 75th percentile, whiskers extend to the most extreme datapoints whereas outliers are plotted individually. The prediction error method has been used as identification algorithm. Actual values are highlighted using horizontal lines.

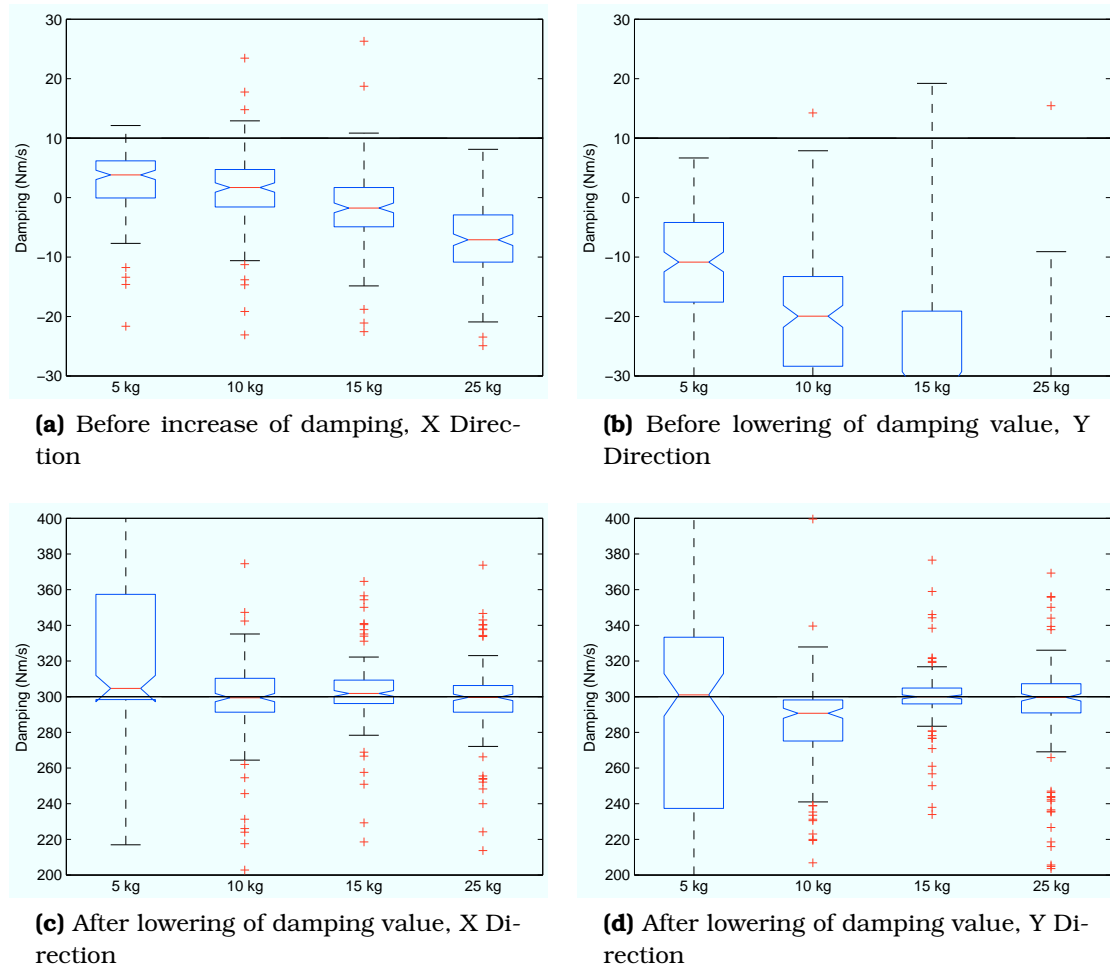


**Figure 4.21.:** Box-whisker plots of estimated damping values in 'Punch Object' task. Central mark is the median, the edges of the box are the 25th and 75th percentile, whiskers extend to the most extreme datapoints whereas outliers are plotted individually. The predication error method has been used as identification algorithm. Actual values are highlighted using horizontal lines.

## 4.5. Physical mass and spring load tasks

In addition to simulated loads, experiments with a physical mass and spring loads have been performed and subsequently evaluated. Section 3.4 briefly describes the measurement protocol. Task performances have not been evaluated during these experiments.

Accelerations were measured whereas velocities and positions are estimated using Euler integration. The estimation accuracy depends on the movement complexity and duration. Relatively large angular velocities cause erroneous orientation estimations and subsequently accumulated in worse estimated velocities and positions.

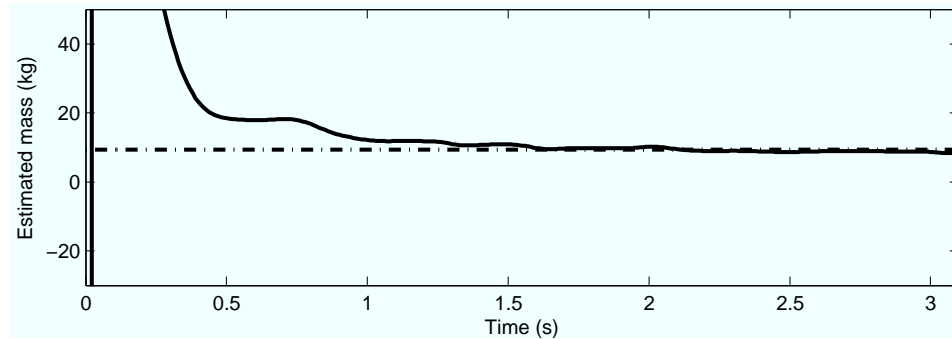
Table 4.2 shows the estimated parameter values of different conditions. Because movements were primary in vertical (z) direction, a one dimensional model has been used. Again the Prediction Error method has been used. When parameter values were known beforehand, error percentages are given too. Variance accounted for (VAF) percentages have been calculated which give an indication how good estimated models fit.

Identification of all conditions resulted in high VAF percentages. The table shows that relatively large movement durations resulted in smaller estimation errors (condition a versus c). Both, mass and spring load condition showed a negative error in estimated and real mass values.

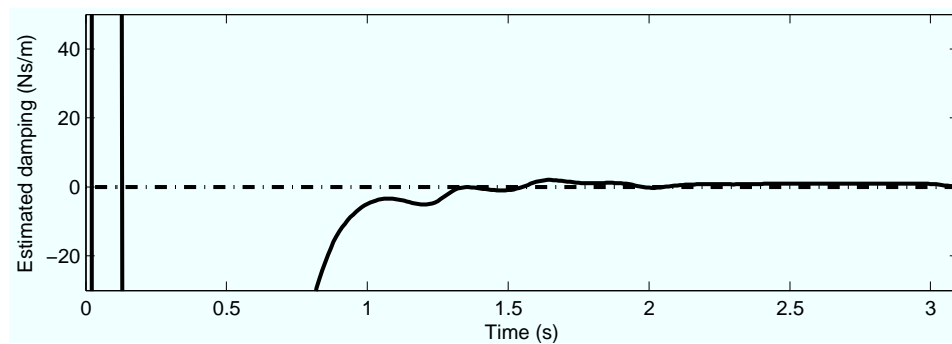
In addition, figure 4.22 shows the recursively identified parameters during a movement of condition a. Visible is that the mass parameter converges to approximately 9.35 kg, and damping and stiffness contributions are negligible.

Load	Movement condition	Duration (s)	Estimated Parameters						VAF Scores (%)
			Mass		Damping		Stiffness		
			(kg)	Err.(%)	(Ns/m)	Err.(%)	(N/m)	Err.(%)	
Mass	a	3.3 ± 0.3	8.9±0.2	-4.2±2.2	0.7±0.6	-	3.2±1.1	-	99.98±0.01
Mass	b	3.5 ± 0.2	9.0±0.1	-3.8±1.4	0.6±2.2	-	0.4±1.5	-	99.94±0.09
Mass	c	4.6 ± 0.6	9.1±0.2	-3.2±2.3	0.1±0.3	-	2.7±2.5	-	99.10±0.28
Spring	d	4.2 ± 0.9	0.9±0.6	-	1.8±2.1	-	85.7±5.1	-2.5 ±5.9	99.65±0.66

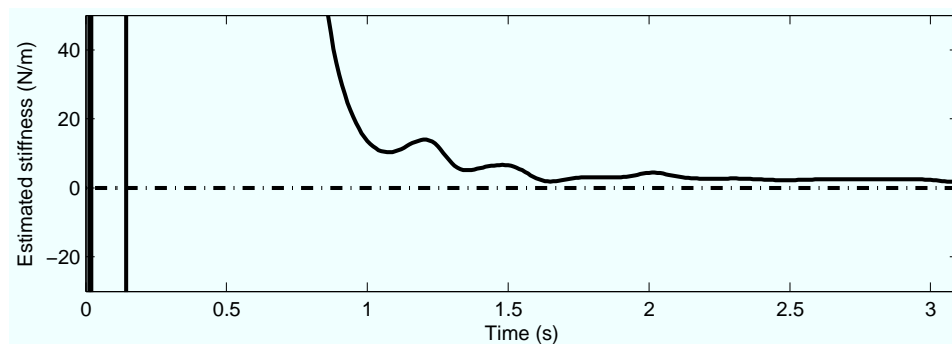
**Table 4.2.:** Estimated parameter values of physical loads. Mean and standard deviations are given for 19 trial repetitions of all movement conditions.



(a) Estimated mass value



(b) Estimated damping value



(c) Estimated stiffness value

**Figure 4.22.:** Recursive identification of parameters values during a displacement of a 9.35 kg mass weight (movement condition a).



## 5. Discussion and Conclusions

This chapter discusses the results, presents the conclusions of work done and give directions for further research. The performed research work shows the feasibility of evaluating functional task performances in daily life situations. In particular we concentrated on arm/hand interactions with environmental loads. Interface measurements of kinetic and kinematic quantities, between hand and load, have been used to quantify the task performance and identify load and body dynamics.

Evaluated human load interactions belong to the class of functional movements with specific criteria and conditions, among which environmental loads have passive loads and behave piece-wise linear. Three hypotheses have been stated and are tested using experimental setups:

- Performance of functional tasks can be evaluated.
- Load dynamics can be identified during stationary periods if perturbation is sufficient.
- Momentary information about human dynamics can be derived from responses to changing load characteristics.

### 5.1. Evaluation of task performance

Task performances have been evaluated while subjects performed three different arm tasks. Movement and force measurements have been used to evaluate criteria of which the subjects were informed before they performed the corresponding task. When the task was performed, the subject was visually informed of their gained score, such that they were immediately able to anticipate during the next trial.

The 'Displace Object' task showed the bell shaped velocity profiles which are typical for reaching movements. Other traditional regularities, and possible trends between subjects and successive trials have not been evaluated.

Regarding the proposed theories of Wolpert et al. (23) (24), that the CNS utilizes an internal model in the control of motor behavior, it would be interesting how the motor commands are affected by sensory inflow of the states (feedback) and feedforward models of the limb dynamics. During the 'familiarization' period of a new task, the (relatively slow) feedback component would have a significant contribution, whereas after this period control relies more on the internal feedforward model.

Patients suffering from movement disorders would have deficits in their internal model (38) which result in abnormal movement trajectories. Suggested interface

sensors could indicate the degraded task performance and perhaps classify the kind of movement disorder.

## 5.2. Identification of load dynamics

Load dynamics were successfully identified in the X direction of the trajectories. The iterative 'Prediction Error' method showed the best results. Error of identified masses were  $3.8 \pm 5.8\%$  for 5 kg and  $0.1 \pm 10.0\%$  for 25 kg simulated inertias during the 'Displace Object' task.

Due to limitations of the haptic robot ('HapticMaster') identification results in Y direction were much less accurate and therefore unreliable. The 'Prediction Error' method identified the 5 kg mass with an error of  $7.2 \pm 17.9\%$  and  $9.1 \pm 21.3\%$  for the simulated 25 kg mass.

Accelerations were not rendered correctly in Y direction which resulted in incorrect movements according simulated load. Especially low accelerated mass movements caused oscillations around 14 Hz, which can be regarded as unstable behavior. Possible reasons would be some misalignment or malfunction of mechanical components. A discussion with the manufacturer of the robot turned out that wear of these components would be a logical explanation. Another reason would be the finite render capabilities of the robot's controller. Of course, this is again dependent of actuators, transmissions and sensors used.

The ARX method showed less accurate estimates ( $6.4 \pm 16.2\%$  for 5 kg and  $1.3 \pm 10.9\%$  for 25 kg) which is probably caused by the model structure. The noise contribution can not be modeled separately from the system model, which resulted in wrong estimates when noise was added to the input of considered model structure (see figure 2.4). Furthermore when noise can not be captured using the defined noise model, like non-linear behavior, a biased estimate will be obtained.

Compared to the other two methods, the subspace method showed a larger variance in estimated parameters (see figure 4.11). As the system output can be described by a variety of A and B matrices (see equation 2.26), a 'sub-optimal' model will be estimated.

The recursive identification algorithm was not able to estimate parameters during the 'HapticMaster' experiments. This can be explained in different ways. First the average duration of interaction was too short in order to provide the identification algorithm a sufficient 'rich' input. This is furthermore dependent on how the movement was performed, e.g. identification was more successful when the load was more dominated by the mass (e.g. 25 kg) and subjects more actively accelerated and decelerated the mass. Unfortunately this was difficult to achieve as the hapticmaster was restricted in maximal applied forces. In addition, recursive methods require some

time to converge the parameters to their estimated values. Finally, the recursive algorithm is a modified version of the ARX method and therefore deals in a similar way with noise contributions.

The other two task conditions employed load discontinuities during the movement. Simulated loads differ before and after this transition and therefore identification algorithms required a separate treatment of both parts. The accuracy of identified dynamics was extremely dependent of the movement duration.

In addition to the 'HapticMaster' experiments, measurements of a previous experiment with physical loads have been evaluated. Identification of mass loads were successful with an estimated mass error between 3 and 4%, while stiffness of the spring load condition was accurately estimated with an error of  $-2.5\%$ . Moreover, identified models show a good fit, i.e. mean VAF percentages where between 99 and 100%.

Furthermore, the physical loads could be successfully identified by the recursive estimation algorithm. This is probably due to longer movement durations, and higher SNR values of measured quantities.

### 5.2.1. Changing load dynamics

System identification algorithms provide more accurate parameter estimates when all observations are available offline. This in contrast to recursive algorithms where parameter estimates are based on observations up to the current time. Advantage of latter method is the possibility of online (varying) parameter estimations. Question is whether this is necessary because offline methods give more accurate estimations and require, in general, less processing time.

Interactions in daily life situations occur often in combination with periodically stationary loads. However, load dynamics can change in time. Two situations should be distinguished. First is a gradually, smoothly change in parameter values. Second is a step like change, i.e. abruptly change in dynamics.

Situations in which dynamics change more gradually include: manipulation of object whose dynamics are dependent of temperature or objects which are subjected to wear (irrelevant for long-term). A more practical example is when someone holds a glass in his/her hand while it is filled by a certain liquid.

Identification of gradually changing parameter changes is possible by a recursive system identification algorithm, as being discussed in the background chapter. Another approach for time dependent models is using a window over the entire measured data set and use conventional non-recursive algorithms. Hence, there will be a trade-off between window length, data length and rate of change in parameter values (17).

However in many daily life situations load dynamics are subjected to abrupt changes.

One could think of: putting objects onto a solid surface, manipulation of switches and doorhandles, throwing objects or using a keyboard.

Identification of such systems is rather difficult, as the choice of update step or 'Gain' in regular recursive algorithms is a tradeoff between tracking ability and noise sensitivity. To track abrupt system changes, using recursive algorithms, a relatively high gain would be required but has the consequence of being sensitive of disturbances in the data.

In 'MATLAB' a so called 'segment' algorithm is available which is specifically designed for tracking abruptly changing systems. It is an modified version of the recursive algorithm (39). By using multiple parallel models which are updated independently, the recursive algorithm is equipped with an update gain which can be adapted every update step.

Another possibility is using a non recursive algorithm in combination with prior knowledge about the onset and duration of jumps in load dynamics. This method is only usable in, generally acceptable, offline situations. Detection of system jumps could be performed by sudden changes in either acceleration or force signals. For example, collision with a stiff object can be detected by the steep decline in measured acceleration. A sudden decline in inertia (throwing an object) could be detected by an increase in acceleration.

Before applying identification algorithms it is essential that the performed task has been classified. Suggested algorithms are only suitable for the specific class of tasks as mentioned in the introduction in this thesis. Other task classes (e.g. maintaining the hand position in space while being disturbed) require a complete different approach.

### 5.2.2. Estimation error analysis

Taking only parametric identification algorithms in consideration, one should select a proper model structure prior to identification process. The best model structure is typically a trade-off between flexibility and parsimony, i.e. the possibility to capture all dynamics of a system versus the essential dynamics.

In this research work, merely second order systems are considered. This is a more parsimonious decision because real loads will not express pure second order dynamics. However the dynamic part which cannot be captured (in case of a second order structure) is of no importance. The essence is whether the system mainly appears to be of inertial, elastic, or dissipative nature in the range of use.

In three dimensional space (translational and rotational), things can get more complicated as coupling exists between axis of motion. For example masses exhibit inertial characteristics during rotational movements.

In addition, it will not be possible to identify the dynamics of both human body and load in their complete working range, since they are physically coupled during the interaction and, therefore, have joint dynamics. Coupling of both systems requires

a closed loop identification approach in order to correctly separate both dynamic contributions. However, the class of daily life interactions, as treated in this research study, are performed using feedforward and open loop control mechanisms of the CNS. When the body perturbs the load by applying forces, information visible on the contact interface is merely a characterization of the load. This allows us to use the open-loop identification algorithms.

In addition it is not necessary to identify loads in their complete working range as they will never express themselves, during interaction, outside the range where the human body is operating.

Summarizing, we are more interested in how well the joint dynamics can be described as being of inertial, elastic or dissipative nature. Hence it is important to know how good mass, stiffness and damping parameters are estimated. Normally prior information of these parameters is unknown, which makes it difficult to evaluate the estimation accuracy. Therefore evaluation of the model output is more common approach.

Different techniques as discussed in section 2.5.5 give valuable information of the probability whether or not the estimated model is a correct mapping of the actual system. VAF percentage scores give an indication of the goodness of model fits. In addition, correlation analysis of residuals give information whether prior assumptions of model order and open or closed loop situations are correct.

Furthermore, trial to trial parameter estimations, during equal stationary conditions, give information about the certainty of estimated values. But this is only applicable when tasks are repeated or have cyclic characteristics, i.e. in ergonomics.

### 5.3. Identification of body dynamics

Load discontinuities gave limited responses of the human body. Force responses were visible in the 'Punch Object' task (sudden rise of damping) for small simulated end effector inertias (5 kg). An oscillation like behavior is noticed after 'collision'. This could be caused by a high muscle stiffness resulting in underdamped behavior. Muscle stiffness is a function of intrinsic musculo-skeletal and reflexive properties. The properties are variant and therefore the body is able to modify stiffness and damping characteristics. Muscle co-contractions are a well described method to increase stiffness. Especially when learning new tasks, the human body applies this mechanism for a successful performance.

Full identification of arm/hand dynamics is impossible as the perturbations are transient-like and therefore too short to qualify and identify both intrinsic and reflexive dynamic contributions. Moreover, perturbations of the body are caused by an abrupt change in load dynamics. In this particular situation the body is operating in closed loop with the environmental load. Information on the interface is a combination of intrinsic dynamics of both load and body and a reflexive force contribution of

the human body (visible after typical reflex delays for the upper limb, 25-30 ms (4)). Erroneous estimates of dynamics will be obtained because the suggested identification algorithms do not assume a closed loop system structure. External known disturbances, combined with a closed loop model structure are required to successfully separated both system dynamics (4) (30).

### **5.3.1. Relation between responses of changing loads and movement control of the human body**

The relation between human body dynamics and their movement control is an interesting topic that follows from this research. Under healthy conditions, humans can adapt their reflexive motor control flexibly and optimally to varying loads, but patients with central neural disorders like stroke are not able to do so (40).

In addition studies have shown that in stroke patients reaching movements are characterized by decreased movement speed and increased movement variability with respect to healthy subjects (41). Reaching task performances will thus be degraded for impaired subjects.

Former studies conclude that post stroke patients show an increases muscle stiffness compared to healthy subjects. This effect is devoted to an increase in reflexive gains (42). Such effects would be visible in force and movement responses when the patient is exposed to changing loads.

## 5.4. Conclusions

- Evaluation of tasks performances is possible using interface force and/or movement measurements.
- Identification of load dynamics using interface measurements is possible under certain conditions: interaction between human body and load occur in open loop and the load must be sufficiently perturbed by the body.
- Momentary information of body dynamics is available on the contact interface when load dynamics suddenly change in time.

## 5.5. Recommendations

A shortlist of recommendations resulting from the discussion is given below:

- **Usage of physical loads instead of simulating loads.** The performance of hapticmaster is insufficient and unreliable. Accelerations are not correctly rendered, while they are of high importance because in many daily lift tasks masses dominate load dynamics.
- **Optimization of identification algorithms** to track load dynamics in short interaction where a minimum amount of information will be available on the contact interface. The algorithm should be 'discontinuity' proof, i.e. it should resist abruptly changing load dynamics, which means that detection of the discontinuity onset is necessary.  
Furthermore, the model structure has to be extended for full 3D dynamics, which means that rotational inertia's should be incorporated.
- **Quantification of momentary information derived from body responses to load perturbations.** This research work showed limited, transient like, responses to changes in load dynamics. Further research of the responses is required for better understanding of underlying intrinsic and reflexive body dynamics.
- **An experimental study with patients having neural disorders like stroke.** Both evaluation of task performances and responses of the body to changing loads would be of great importance to show the significance of sensing on interface of human body and load.



# A. HapticMASTER related

## A.1. Control interface window

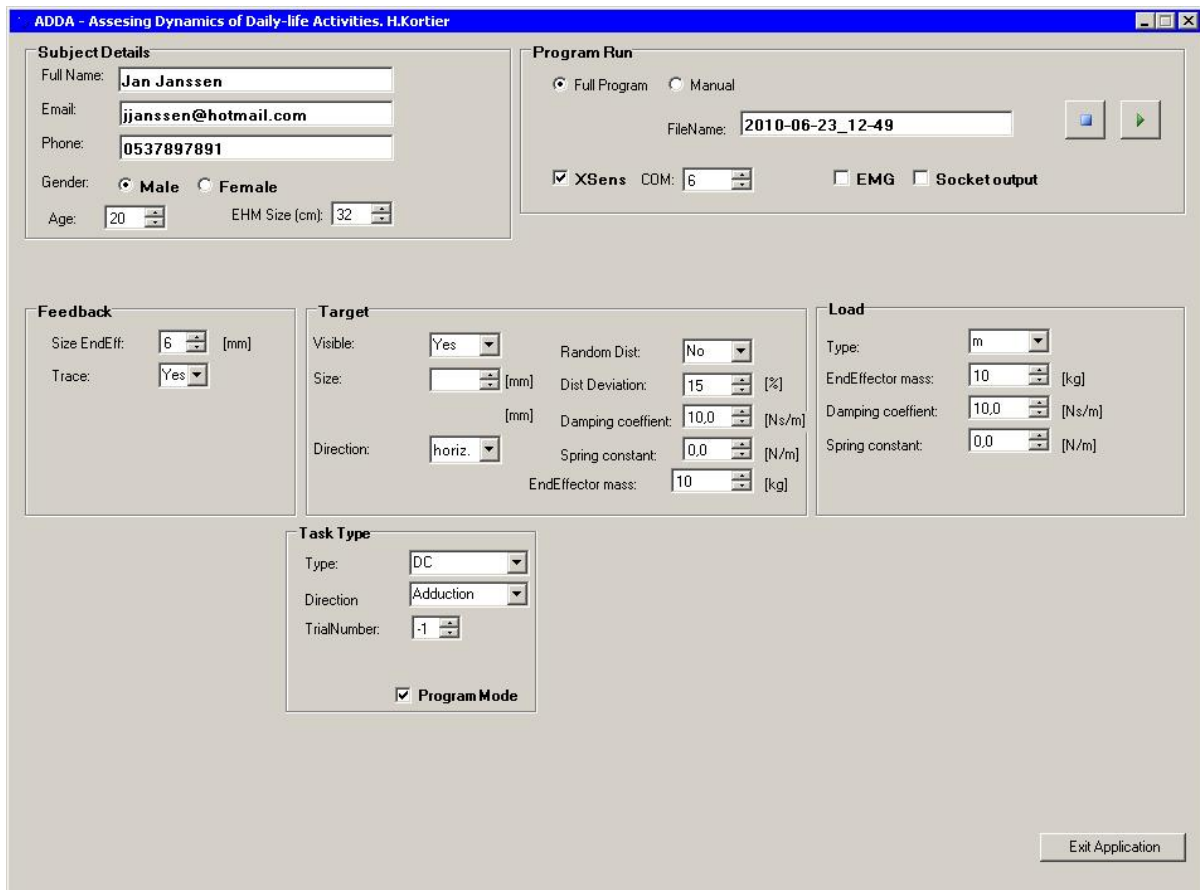


**Figure A.1.:** Control Interface used for controlling hapticmaster and xsens hardware. In addition it provides signal acquisition of both devices

## A.2. HapticMASTER Specifications

General		Haptics	
Control type	Admittance	Position resolution	$4 \times 10^{-6}$ [m]
Active DoF	three (x,y,z)	Force sensitivity	0.01 [N]
Power	500 [W]	Nominal output force	100 [N]
Voltage	90-264 [VAC]	Maximum output force	250 [N]
Console height	0.8 [m]	Minimal simulated inertia	2 [kg]
		Maximum simulated stiffness	$5 \times 10^4$ [N/m]
		Maximum velocity	1.0 [m/s]
		Maximum deceleration	50 [m/s <sup>2</sup> ]

**Table A.1.:** HapticMASTER specifications

## B. Additional information

### B.1. Derivation of vd Helm's upper arm model

First the intrinsic arm mass, damping and stiffness:

$$H_i(s) = \frac{X_a(s)}{F_{int}(s)} = \frac{1}{m_a s^2 + b_a s + k_a} \quad (\text{B.1})$$

Transfer of the hand dynamics are function of an elastic ( $k_h$ ) and viscous component ( $b_h$ ).

$$H_h(s) = \frac{F_h(s)}{X_h(s) - X_a(s)} = b_h s + k_h \quad (\text{B.2})$$

The intrinsic arm model becomes ( $F_{int}(s) = F_h(s)$ ):

$$\frac{X_h(s)}{F_h(s)} = \frac{1 + H_h(s)H_i(s)}{H_h(s)} = H_h^{-1}(s) + H_i(s) \quad (\text{B.3})$$

Reflexive length and velocity feedback including muscle activation, with neural delay  $T_d = 25 \text{ ms}$

$$H_r(s) = \frac{A(s)}{X_a(s)} = (k_v s + k_p) e^{-T_d s} \quad (\text{B.4})$$

Muscle activation dynamics with time constant  $\tau_a = 30 \text{ ms}$

$$H_{act}(s) = \frac{1}{\tau_a s + 1} \quad (\text{B.5})$$

Intrinsic arm (without hand dynamics) and reflexive feedback can now be formulated as

$$H_a(s) = \frac{X_a(s)}{F_f(s)} = \frac{H_i(s)}{1 + H_i(s)H_r(s)H_{act}(s)} \quad (\text{B.6})$$

which forms the feedback path to the hand dynamics  $H_h(s)$ , resulting in the arm dynamics (including the hand)

$$H_{arm}(s) = \frac{X_h(s)}{F_h(s)} = H_h^{-1}(s) + H_a(s) \quad (\text{B.7})$$

## B.2. Kalman Approach for recursive identification

The linear regression model can be cast into the form of a state space equations:

$$\begin{aligned}\theta(t+1) &= \theta(t) \\ y(t) &= \varphi^T(t)\theta(t) + v(t)\end{aligned}\tag{B.8}$$

Now we postulate that the parameter vector  $\theta$  is not constant but varies like a random walk:

$$\theta(t+1) = \theta(t) + w(t) \quad Ew(t)w^T(w) = R_1(t)\tag{B.9}$$

where  $w$  is white Gaussian and  $E v^2(t) = R_2(t)$ . Now the Kalman filter approach gives the expectation and covariance of  $\hat{\theta}$  as:

$$\hat{\theta}(t) = \hat{\theta}(t-1) + L(t) \left[ y(t) - \varphi^T(t)\hat{\theta}(t-1) \right]\tag{B.10}$$

$$L(t) = \frac{P(t-1)\varphi(t)}{R_2(t) + \varphi^T(t)P(t-1)\varphi(t)}\tag{B.11}$$

$$P(t) = P(t-1) + R_1 - \frac{P(t-1)\varphi(t)\varphi^T(t)P(t-1)}{R_2(t) + \varphi^T(t)P(t-1)\varphi(t)}\tag{B.12}$$

# References

- [1] ATI. **Force sensors**. <http://www.ati-ia.com/products/ft/sensors.aspx>. 3
- [2] D ROETENBERG, P.J SLYCKE, AND P.H VELTINK. **Ambulatory position and orientation tracking fusing magnetic and inertial sensing**. *IEEE transactions on biomedical engineering*, **54**(5):883–890, Jan 2007. 3
- [3] L. LJUNG AND E.J. LJUNG. *System identification: theory for the user*. Prentice-Hall Englewood Cliffs, NJ, 1987. 3, 16, 17
- [4] FCT VAN DER HELM, AC SCHOUTEN, E DE VLUGT, AND GG BROUWN. **Identification of intrinsic and reflexive components of human arm dynamics during postural control**. *Journal of neuroscience methods*, **119**(1):1–14, 2002. 4, 8, 21, 72
- [5] RE KEARNEY, RB STEIN, AND L PARAMESWARAN. **Identification of intrinsic and reflex contributions to human ankle stiffness dynamics**. *IEEE Transactions on Biomedical Engineering*, **44**(6):493–504, 1997. 4, 9, 21
- [6] KONRAD P KÖRDING AND DANIEL M WOLPERT. **Bayesian integration in sensorimotor learning**. *Nature*, **427**(6971):244–7, Jan 2004. 4, 12
- [7] E TODOROV AND MI JORDAN. **Optimal feedback control as a theory of motor coordination**. *Nature neuroscience*, **5**(11):1226–1235, 2002. 4, 12
- [8] EMANUEL TODOROV. **Optimality principles in sensorimotor control**. *Nature neuroscience*, **7**(9):907–15, Sep 2004. 8, 12
- [9] E TODOROV. **Stochastic optimal control and estimation methods adapted to the noise characteristics of the sensorimotor system**. *Neural computation*, **17**(5):1084–1108, 2005. 8, 12
- [10] DM WOLPERT. **Probabilistic models in human sensorimotor control**. *Human movement science*, **26**(4):511–524, 2007. 8
- [11] ERWIN DE VLUGT, ALFRED C SCHOUTEN, AND FRANS C T VAN DER HELM. **Adaptation of reflexive feedback during arm posture to different environments**. *Biological cybernetics*, **87**(1):10–26, Jul 2002. 8
- [12] EJ PERREULT, RF KIRSCH, AND AM ACOSTA. **Multiple-input, multiple-output system identification for characterization of limb stiffness dynamics**. *Biological cybernetics*, **80**(5):327–337, 1999. 9
- [13] E DE VLUGT, AC SCHOUTEN, AND FCT VAN DER HELM. **Closed-loop multivariable system identification for the characterization of the dynamic arm compliance using continuous force disturbances: a model study**. *Journal of neuroscience methods*, **122**(2):123–140, 2003. 9
- [14] AJ PICK AND DJ COLE. **Dynamic properties of a driver's arms holding a steering wheel**. *Proceedings of the Institution of Mechanical Engineers, Part D: Journal of Automobile Engineering*, **221**(12):1475–1486, 2007. 9
- [15] YANGMING XU AND J.M HOLLERBACH. **Identification of human joint mechanical properties from single trial data**. *Biomedical Engineering, IEEE Transactions on DOI - 10.1109/10.704874*, **45**(8):1051–1060, 1998. 9
- [16] Y XU AND JM HOLLERBACH. **A robust ensemble data method for identification of human joint mechanical properties during movement**. *IEEE transactions on biomedical engineering*, **46**(4):409–419, 1999. 9
- [17] KONCZAK J AND BROMMANN K. **Identification of Time-Varying Stiffness, Damping, and Equilibrium Position in Human Forearm Movements**. *Motor Control*, pages 1–20, Apr 2002. 9, 69
- [18] E TODOROV AND M.I JORDAN. **Smoothness maximization along a predefined path accurately predicts the speed profiles of complex arm movements**. *Journal of Neurophysiology*, **80**(2):696–714, Jan 1998. 10, 11
- [19] A. SHUMWAY-COOK AND M.H. WOOLLACOTT. *Motor control: translating research into clinical practice*. Lippincott Williams & Wilkins, 2006. 10
- [20] F. LACQUANTI, C. TERZUOLO, AND P. VIVIANI. **The law relating the kinematic and figural aspects of drawing movements**. *Acta Psychologica*, **54**(1-3):115–130, 1983. 11
- [21] T FLASH AND N HOGAN. **The coordination of arm movements: an experimentally confirmed mathematical model**. *J Neurosci*, **5**(7):1688–703, Jul 1985. 11
- [22] Y UNO, M KAWATO, AND R SUZUKI. **Formation and control of optimal trajectory in human multijoint arm movement**. *Biological cybernetics*, **61**(2):89–101, 1989. 11
- [23] DM WOLPERT, Z GHAHRAMANI, AND MI JORDAN. **An internal model for sensorimotor integration**. *Science*, **269**(5232):1880, 1995. 11, 67
- [24] DM WOLPERT AND CM HARRIS. **Signal-dependent noise determines motor planning**. *Nature*, **394**:780–784, Aug 1998. 12, 67
- [25] S.H. SCOTT. **Optimal feedback control and the neural basis of volitional motor control**. *Nature Reviews Neuroscience*, **5**(7):532–546, 2004. 12
- [26] DM WOLPERT AND Z GHAHRAMANI. **Bayes rule in perception, action and cognition**. *The Oxford Companion to the Mind*. Oxford University Press (<http://eprints.pascal-network.org/archive/00001354/>), 2005. 12
- [27] L LJUNG AND T SÖDERSTRÖM. *Theory and practice of recursive identification*. Prentice Hall PTR, 1983. 16, 18, 22
- [28] T. KATAYAMA. *Subspace methods for system identification*. Springer Verlag, 2005. 18
- [29] R.G.K.M AARTS. **System identification course.**, 2007. 18
- [30] H VAN DER KOOIJ, E VAN ASSELDONK, AND FCT VAN DER HELM. **Comparison of different methods to identify and quantify balance control**. *Journal of neuroscience methods*, **145**(1-2):175–203, 2005. 22, 72
- [31] N HOGAN. **The mechanics of multi-joint posture and movement control**. *Biological Cybernetics*, **52**(5):315–31, Jan 1985. 22
- [32] H. GARNIER AND L. WANG. *Identification of continuous-time models from sampled data*. Springer, 2008. 23
- [33] MOOG. **HapticMASTER**. [urlhttp://www.moog.com](http://www.moog.com). 29, 30
- [34] SENSABLE. **PHANTOM**. <http://www.sensable.com/>. 30
- [35] RQ VAN DER LINDE, P. LAMMERTSE, E. FREDERIKSEN, AND B. RUITER. **The HapticMaster, a new high-performance haptic interface**. In *Proc. Eurohaptics*, pages 1–5. Citeseer, 2002. 30, 41
- [36] W.E. GARRETT AND D.T. KIRKENDALL. *Exercise and sport science*. Williams & Wilkins, 2000. 31
- [37] P.H VELTINK, H KORTIER, AND H.M SCHEPERS. **Sensing Power Transfer Between the Human Body and the Environment**. *Biomedical Engineering, IEEE Transactions on*, **56**(6):1711–1718, 2009. 38
- [38] R.F BEER, J.P.A DEWALD, AND W.Z RYMER. **Deficits in the coordination of multijoint arm movements in patients with hemiparesis: evidence for disturbed control of limb dynamics**. *Experimental Brain Research*, **131**(3):305–319, Jan 2000. 67
- [39] P. ANDERSSON. **Adaptive forgetting in recursive identification through multiple models**. *International Journal of Control*, **42**(5):1175–1193, 1985. 70
- [40] AC SCHOUTEN, W.J.T. VAN DE BEEK, JJ VAN HILTEN, AND F.C.T. VAN DER HELM. **Proprioceptive reflexes in patients with reflex sympathetic dystrophy**. *Experimental Brain Research*, **151**(1):1–8, 2003. 72
- [41] MC CIRSTEA AND MF LEVIN. **Compensatory strategies for reaching in stroke**. *Brain*, **123**(5):940, 2000. 72
- [42] L. GALIANA, J. FUNG, AND R. KEARNEY. **Identification of intrinsic and reflex ankle stiffness components in stroke patients**. *Experimental Brain Research*, **165**(4):422–434, 2005. 72